Development of a Double-Ended Gauge Block Interferometer for Measurement of the Absolute Length

Von der Fakultät für Elektrotechnik, Informationstechnik, Physik
der Technischen Universität Carolo-Wilhelmina
zu Braunschweig

zur Erlangung des Grades eines
Doktors der Naturwissenschaften
(Dr.rer.nat.)
genehmigte
D i s s e r t a t i o n

von Amany Abdelaty Mohammed Abdelnaser
aus Kairo, Ägypten

1. Referent: Prof. Dr. Peter Lemmens

2. Referent: Prof. Dr.-Ing. Rainer Tutsch

eingereicht am: 26. Januar 2012

mündliche Prüfung (Disputation) am: 29. Februar 2012

Druckjahr: 2012

To my father

Acknowledgments

First of all whole praise is to **ALLAH**, the lord of the world, the source of all knowledge, the knower of everything, and who pleased me to finish this work during the period from 2007 to 2012 at the Physikalisch-Technische Bundesanstalt (PTB), Germany.

I am heartily thankful to **Dr. Renè Schödel**, head of the Interferometry on Material Measures Department at Physikalisch-Technische Bundesanstalt (PTB), for his innovative and constructive ideas that led to this research topic. He follows my work almost day by day with his valuable comments, ideas, and guidance throughout the course of the study.

From the depth of my heart, I am greatly indebted to **Prof. Dr. Peter Lemmens**, the head of Institute for Condensed Matter Physics of the Technical University of Braunschweig, whose encouragement and support from the preliminary to the concluding level enabled me to develop an understanding of the subject.

I would like to express my deepest thanks to **Prof. Dr.-Ing. Rainer Tutsch**, head of the Institute for Production Measurement Technology of the Technical University of Braunschweig, for his continuous supervision and assistance's during my thesis.

I would like also to express my deepest thanks to **Dr. Ahmed Abou-Zeid**, previous head of the Interferometry on Material Measures Department at PTB, for his support and encouragement even after his retirement.

Sincerely thanks to **Dipl.-Ing. Peter Franke**, head of the interferometric calibration of gauge blocks group at PTB, for sharing his experimental knowledge. Special thanks to **Dipl.-Ing. Alexsander Walkov** for his assistance in programming, **Mr. Frank Lechelt**, **Mr. Hans-Henning Ernst** for the measurement of the surface roughness and INKO5 and Köster measurements and **Mr. Alexander Eitz** for designing mechanical components. I wish also to convey my gratitude to **my colleagues at precision engineering division of PTB** for providing a good working atmosphere, and for sharing their scientific knowledge.

Great thanks also to the **international graduate school of metrology** (IGSM) in Braunschweig for the useful metrological lectures during my thesis and continuous help and support.

I am deeply thankful and profoundly grateful to **my parents**, **my husband (Ahmed Salama)**, **my daughter** (**Noreen**), **my son** (**Yasin**), **my sisters** and **my brothers** for their love, care, pray, support, help, patience, and encouragement during the study period. Without them, I would have never the chance to achieve lots of things.

Finally, Great thanks to the **Egyptian culture affair and mission sector**, under the Egyptian government, for supporting me financially during the study period, also great thanks for my institute in Egypt, the **National Institute of Standards** (NIS), for selecting me to take this scholarship.

Vorveröffentlichungen der Dissertation

Teilergebnisse aus dieser Arbeit wurde mit Genehmigung der Fakultät für Elektrotechnik, Informationstechnik, Physik, vertreten durch den Mentor Prof. Dr. Peter Lemmens, in folgenden Beiträgen vorab veröffentlicht:

1- Amany Abdelaty, Alexander Walkov, Peter Franke and René Schödel, “Challenges on double ended gauge block interferometry unveiled by the study of a prototype at PTB”, Metrologia 49 (2012) 1–8.

2- Amany Abdelaty, Alexander Walkov, Ahmed Abou-Zeid and René Schödel, “PTB’s Prototype of a Double-Ended Interferometer for Measuring the Length of Gauge Blocks”, Symposium of metrology 2010 – CENAM, Queretero, Mexico.

Table of Contents

Chapter 1

Introduction

1.1 Motivation

Gauge blocks (GBs) are very important material standards that provide industry with reliable and traceable standards of length. At the highest accuracy, the measurement of GBs must be performed by interferometry.

The conventional method, single-ended interferometer (SEI), to measure the length of GBs is realized with a modified Michelson or Köster interferometer and the GB wrung to an auxiliary platen is required. The Wringing procedure can cause scratches and permanent damage to GB's faces so its measured lengths are affected.

The double-ended interferometer (DEI) offers an alternative design for traceable measurements of the absolute length of GB shaped objects without the need of a platen to be wrung to one of the faces. Thus, both measuring surfaces of a GB are viewed directly. The DEI can open new concepts for absolute length measurements for special applications. The absence of platens to be attached to GBs has definite advantages, e.g. a platen flexing that is observed in thermal expansion measurements, which has to be corrected otherwise, is avoided. Another possible application may be long-term stability measurement of the length of GBs. Using SEIs for such purposes requires the wringing of platens to be maintained all the time, otherwise, i.e. when the wringing has to be renewed, the length is affected by the individual wringing contact. In spite of these advantages, until now, there does not exist a well established DEI-system at any National Metrology Institute (NMI).

This work describes a prototype DEI that was built in Physikalisch-Technische Bundesanstalt (PTB) in order to measure the lengths of GBs in air using two stabilized wavelengths.

1.2 Overview of the Thesis

First, this chapter presents the definition of length metrology and the traceability chain of length measurements.

In chapter 2, the basic principle of length measurement and the GB interferometer systems are presented. The conventional interferometric methods, SEI, and the new method, DEI, are demonstrated. A brief history of the DEI is given. The corrections added to the DEI measurement results are determined.

Chapter 3 involves the description of the overall design of the DEI together with some more detailed aspects such as the two frequency stabilized lasers, the fiber, the optics and the mechanics. The DEI itself is a collection of many components ranging from simple lenses and mirrors to the computer system which controls the entire measurement procedure.

The theory and the measurement method are described in chapter 4. The data analysis and information processing are covered. Phase stepping interferometry (PSI) is used. An example for measurement method steps of a steel GB using Visual Basic 6 is given.

In chapter 5, the uncertainty evaluation in the length measurement of GB by the DEI is evaluated by considering the International Organization for Standardization (ISO) “Guide in the Expression of Uncertainty in Measurement (GUM)”. The influence parameters and the combined

uncertainty calculations are determined. The uncertainty budget is given in a table.

The performance of the DEI-system is presented in chapter 6. It includes results of length measurement over a wide range of lengths (short and long GBs). A comparison of measurements with other PTB comparators is reported. Phase correction is determined using the pack method.

Finally, summary and outlook are presented in chapter 7.

1.3 Length Metrology

Metrology is defined by the International Bureau of Weights and Measures (BIPM) as “the science of measurement and its applications, embracing both experimental and theoretical determinations at any level of uncertainty in any field of science and technology” [1]. It also deals with the basic principles governing quantities and their units. It establishes the international standards for measurement used in the world in science and industry, e.g. distance, time, mass and temperature.

Length is probably considered as the most often measured physical parameter. The dimensional metrology field consists of three branches which are linear metrology (one-dimensional length measurements), geometrical metrology (multi-dimensional measurements) and angular metrology (measurement of angles) [2].

The first civilization who knew how to develop a standard measurement for length was the ancient Egypt. This was called the Cubit. This Royal Egyptian Cubit was based on the length of the Pharaoh’s arm. A master copy of this

measure was carved into a block of granite and its copies of measuring sticks had to be re-calibrated against the royal standard every month.

Figure 1.1 Egyptian cubit rule of 0.52 m, source: [3].

1.4 Brief History of the Meter Definition

The current definition of the meter is "the length of the path travelled by light in vacuum during a time interval of 1/299 792 458 of a second" [5]. This definition allows the SI unit of length to be reproduced in any laboratory with high accuracy.

The first definition of meter goes back to 1889 when the 1st General Conference on Weights and Measures (CGPM) [6] defined the Prototype Meter as the distance between two lines on a standard bar of an alloy of platinum with ten percent iridium, measured at the melting point of ice.

In 1927 the 7th CGPM adjusted a new definition [7] of the meter to be the distance, at 0 C, between the axes of the two central lines marked on the prototype bar of platinum-iridium, deposited in the BIPM, this bar being subject to one standard atmosphere of pressure and supported on two cylinders of less than one centimeter diameter, symmetrically placed in the same horizontal plane at a distance of 571 millimeters from each other.

In 1960 the 11th CGPM defined the meter to be equal to 1 650 763 73 wavelengths in vacuum of the radiation corresponding to the transition between the $2p^{10}$ and $5d^5$ quantum levels of the krypton-86 atom [8].

By the 1970's a number of wavelengths of stabilized lasers were considered much better sources of light than krypton red-orange. Therefore, the 17th CGPM in 1983 proposed a new definition for the meter [6]. This definition was chosen to be intelligible and understood by physics students and be precise enough to allow metrologists working at the measurement. Hence this definition was kept as simple as possible, with an extra recommendation of how to use it in practice [6]:

"The meter is the length of the path travelled by light in vacuum during a time interval of 1/299 792 458 of a second"

"The definition of the meter in use since 1960, based on the transition between the two lines $2p^{10}$ and $5d^5$ of the krypton atom, is abrogated."

Thus given the defined speed of light, the wavelength of the light can be calculated and a meter can be obtained by counting wavelengths of the light in interferometric measurements [4].

1.5 Length Standards

Line standards and end standards are the two types of length standard. Survey tapes and rulers are examples of line standards. Examples of end standards are GBs and length bars [2].

Line standards are usually measured using an instrument which works as a travelling microscope which traverses the distance between two or more lines

marked on the standard. Line standards range from 1 μm size of micro-lithographic standards up to 50 m survey tapes.

End standards have flat and polished end faces. The length of the end standard is the separation between the end standard faces. PTB is using mechanical probes or interferometrically techniques for doing calibrations of end standards.

1.6 Gauge Blocks

The GBs have rectangular shape. The dimensions of cross-section are fixed, however the nominal lengths of them can be various. The dimensions of GBs are 35 mm × 9 mm or 9 × 30 mm.

(a) (b)

Figure 1.2 GB, (a) a GBs set, (b) Dimensions of the GB.

The GBs nominal length is from 0.5 mm to 1000 mm in length. GBs over 100 mm are supported horizontally at two points apart. These points are termed the ‘Airy points’ each at a distance of 0.211 times the nominal length from the ends of the GB and their positions are stamped on the GB’s surface by the manufacturers. Without supporting the GB at the Airy points, the GB will suffer from prismatic compression under the effect of its weight when standing vertically or from sagging when lying horizontally [4].

Materials of the GBs are steel, tungsten carbide, chromium carbide, ceramic, and cervit with the following thermal expansion coefficients (ppm/°C): 11.7, 4.23, 8.5, 9.5, and 0.2 respectively. In spite of the large thermal expansion coefficient of steel, it is the material of choice for GBs. This is because most measuring and manufacturing machines are made of steel.

The GBs manufacture grades are according to the deviation from flatness and the deviation from parallelism of the measurement surface. There are four tolerance grades; K (00), 0, 1, and 2. Grades K and 0 GBs are generally used as calibration masters since they have lengths very close to their nominal lengths values. Grades 1 and 2 are of higher length tolerance and are used for measurement purposes. GBs made to lower accuracy grades are not usually suitable for measurement by interferometry.

1.7 Traceability Chain of Length Measurements

The international vocabulary of basic and general terms in metrology defines traceability as “the property of a measurement result or the value of a standard whereby the result can be related to a stated reference through a documented

unbroken chain of calibrations, each contributing to the measurement uncertainty" [1].

GBs which measured in terms of wavelength of stabilized lasers can be used to calibrate the lengths of other standards through comparison, i.e. the length is transferred from the calibrated objects to customer objects in industrial applications.

At NMIs, the GBs can be calibrated interferometrically with the smallest possible measurement uncertainties. Thus NMIs are placed at the head of the chain traceability of GB length measurement. Figure 1.3 shows the chain of traceability for GB length measurement from NMIs then, accredited calibration laboratory, up to the users in industry and research.

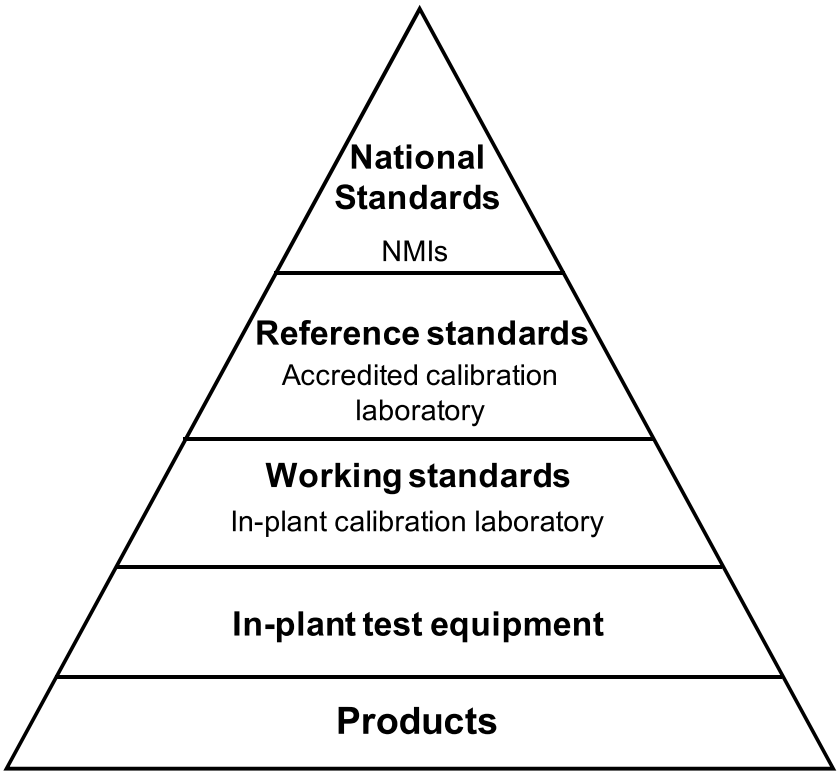

Figure 1.3 Traceability chain for measurement of GB length.

Chapter 2

Gauge Block Length Measuring Interferometers

The GB length measuring interferometers are divided into two different designs:

1) single-ended interferometer, SEI, which based on the Twyman-Green interferometer design. One of the measuring surfaces of the GB should be joint to an auxiliary platen which has reflecting surfaces [5]. This procedure is called ‘wringing’ and the two faces are rotated slowly against each other.

2) double-ended interferometer, DEI, in which both measuring surfaces of a GB are viewed directly without an auxiliary platen.

Before going into more details about the two methods, the principle of the length measurements will be presented.

2.1 Basic Principle of Length Measurements

In general, the basic interferometric principle of length measurement is the comparison of a mechanical length (or a distance in space) against a known wavelength of light:

$$l = \lambda (i + q) \ , \tag{2.1}$$

where l is the length being measured, λ is the wavelength, i is an integer and q is a fraction ($0 < q < 1$). Commonly the optics are arranged in a double-pass system, in this case the measurement units, fringes, are half-wavelengths:

$$l = \frac{\lambda}{2}(i + q) \ . \tag{2.2}$$

2.2 Single-Ended Interferometers (SEI)

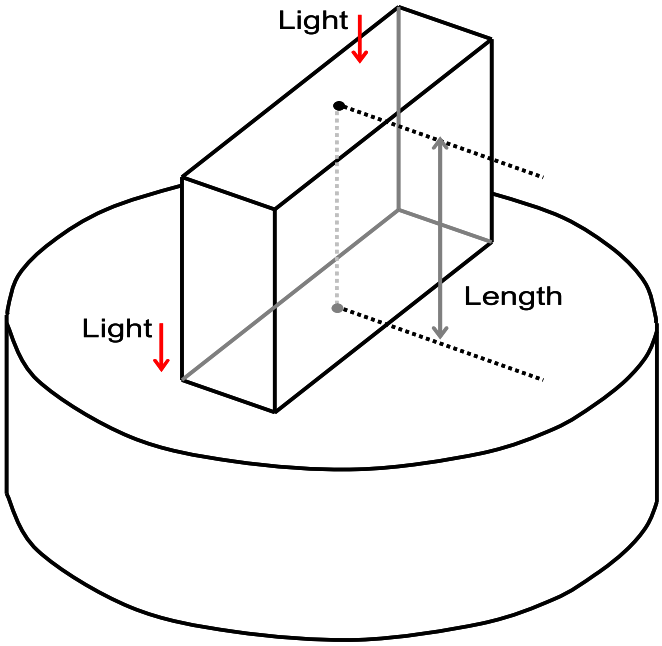

Figure 2.1 The central length of a GB obtained through a single-ended interferometer.

In the modified Michelson and Köster GB interferometers, the GB requires to be wrung onto an auxiliary platen as shown in Figure 2.1. The measured length of a GB is the distance between its one measuring face and the surface of an auxiliary platen on which the other measuring face of the GB has been joined. The beam will be reflected off one end of the GB and the platen surface.

2.2.1 Twyman-Green Interferometer

The Twyman-Green interferometer is a Michelson interferometer with a collimated beam [9]. Using a beam splitter, the beam is divided into two beams, one reaching a reference mirror and the other to a GB attached to a platen. Each beam is reflected and split again at the beam splitter resulting in an interference.

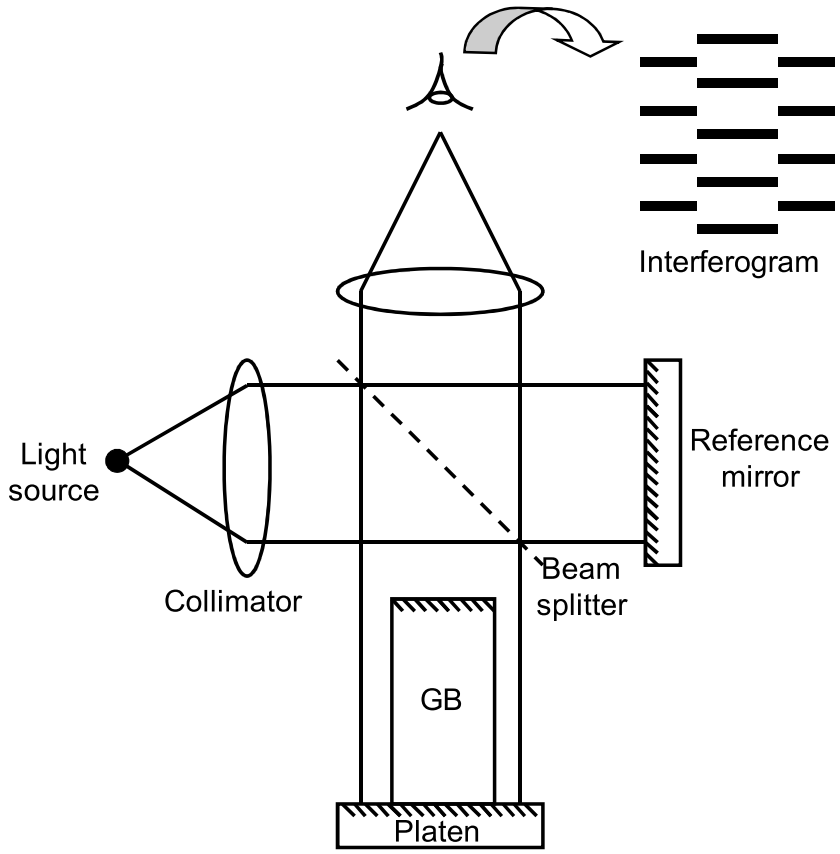

Figure 2.2 Schematic diagram of Twyman-Green interferometer.

2.2.2 Köster Interferometer

The Köster's interference comparator uses a Köster prism which acts as beam splitter [10]. Such type of a design, see Figure 2.3, is particularly useful for length measurements of relatively long GBs.

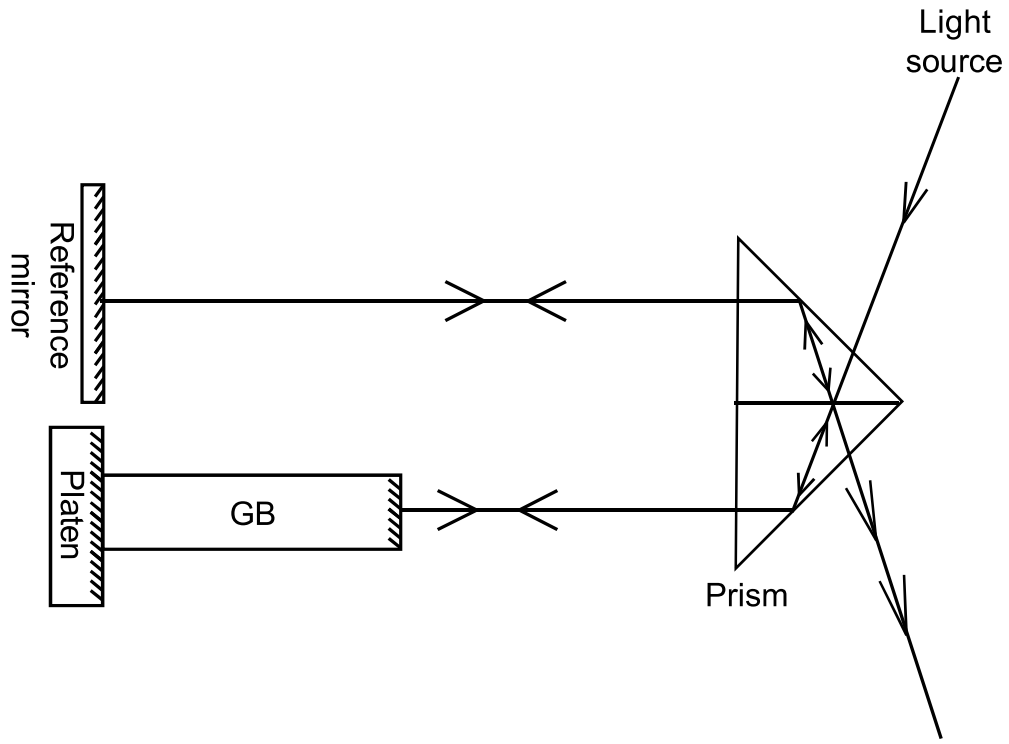

Figure 2.3 Schematic diagram of Köster interferometer.

2.3 Double-Ended Interferometers (DEI)

Because the measurement of a GB using the DEI does not require an auxiliary platen, in this case the measured length of the GB is the distance between the two faces of the GB as shown in Figure 2.4. Thus, by measuring the length of the GB without being wrung to a platen, the beam will be reflected off both faces of the GB.

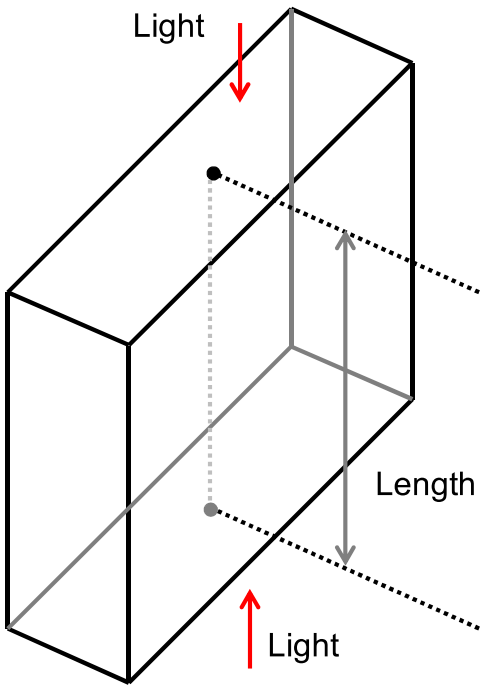

Figure 2.4 The central length of a GB obtained through a double-ended interferometer.

2.4 History of the Double-Ended Interferometer

2.4.1 Dowell End-Gauge Interferometer

The first DEI was already patented and built by Dowell in 1943 [11]. The end-gauge interferometer was made to make comparison between two GBs, G_1 (the standard) and G_2 (unknown GB of the same nominal length) as shown in Figure 2.5.

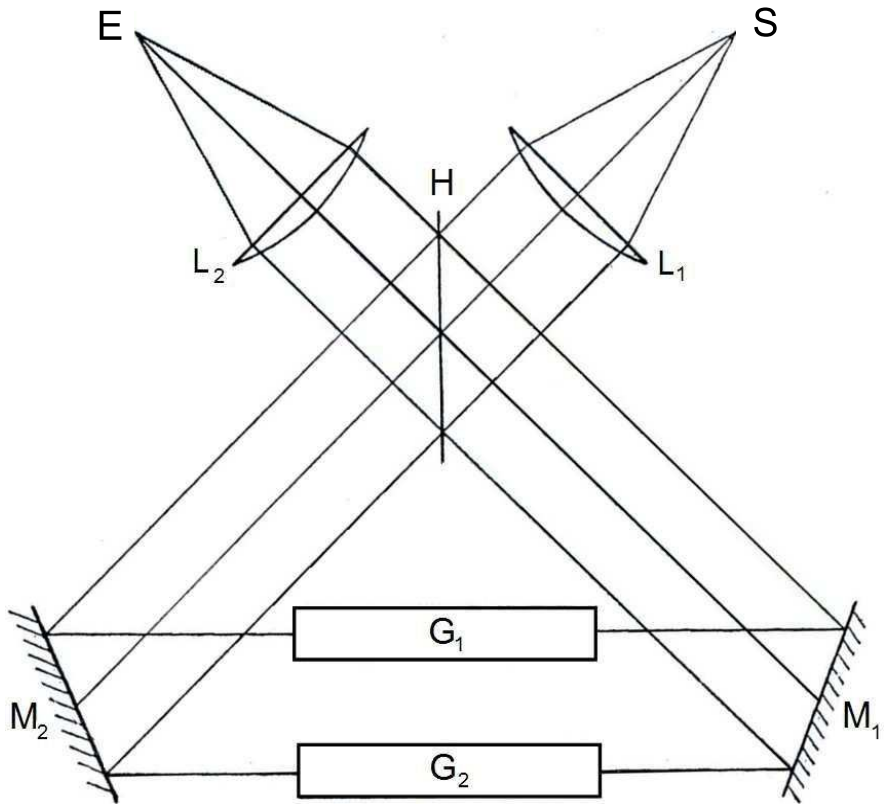

Figure 2.5 Dowell end-gauge interferometer arrangement, source: [11].

In this setup two interfering beams traverse the same path in opposite directions. The light from the source S to the collimator lens L_1, parallel beam, is send to the half-silvered plate H then to the fully silvered mirrors M_1 and M_2. The light from M_1 is reflected from one end of the two GBs, and light from M_2 is reflected from the opposite end, both beams travel back along their own paths and recombine at H. An eye placed at E sees the two GBs side by side.

To obtain white light fringes, the two paths from H to the ends of the GB must be equal. In this critical adjustment, the difference in lengths between the two GBs can be evaluated in terms of wavelengths. Figure 2.6 shows the

interference pattern of the Dowell interferometer. To make the diagram clearer, one pair of images is set higher than the other however, in actual use they would be brought to the same horizontal plane.

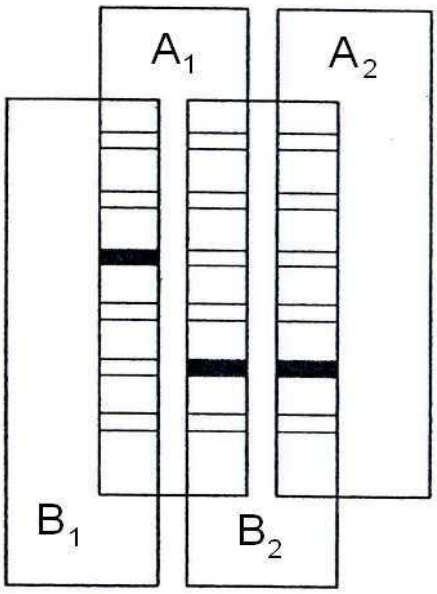

Figure 2.6 Field of view of a Dowell end-gauge interferometer. A_1 and A_2 are coplanar, but B_1 is separated from B_2 by two half wavelengths, source: [11].

2.4.2 Hariharan Interferometer

In 1958, P. Hariharan and D. Sen working at the National Physical Laboratory of India designed an interferometer for the absolute length measurement of long GBs [12]. Other advantages of the instrument are its simplicity of operation and its compact layout. Hariharan suggested a DEI in which the beam traverses two triangular pathways as shown in Figure 2.7.

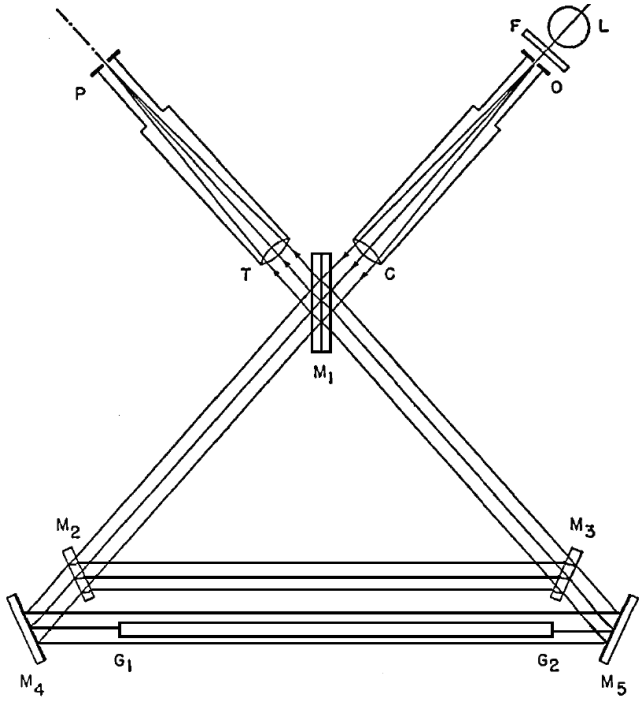

Figure 2.7 Schematic diagram of the interferometer. L, monochromatic light source; O, pinhole; C, collimator; M_1, beam splitter; M_2, M_3, semi-reflecting mirrors; M_4, M_5 mirrors; G_1, G_2, GB; T, telescope objective; P, exit stop, source: [12].

The set up of the interferometer was as follows. Using a large aperture at O, and a suitable monochromatic source, the beam splitters, M_3 and M_2, were first adjusted with the outer path blocked so that the shear fringes can be seen with an eyepiece at P. Next, the mirrors, M_4 and M_5, were adjusted similarly, with the inner path blocked. On replacing the large aperture with a small pinhole, the fringes due to interference between the outer path and the inner path could be seen with the eye placed at P. The GB was then introduced in the outer path and adjusted with the inner path temporarily blocked so that with a white light source the zero order bright fringe covered the end faces. On replacing the white light source with the monochromatic source, and admitting light to

the reference path once again, fringes could then be observed as in Figure. 2.8. The fractional interference order displacement could be estimated.

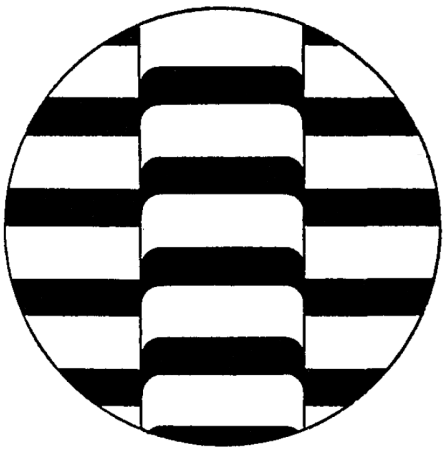

Figure 2.8 The fringe system appearing in the interferometer, source: [12].

2.4.3 Dorenwendt Interferometer

After the invention of the laser, in 1972 Dorenwendt suggested a double-ended design that was based on the extension of a Twyman-Green interferometer in which the absolute length of GBs could be measured without the need for wringing a platen onto one of the end faces [13].

The interferometer consists of a Michelson interferometer connected to additional mirrors, forming a triangularly closed path. In this design, four additional surfaces are introduced increasing the complexity of the alignment.

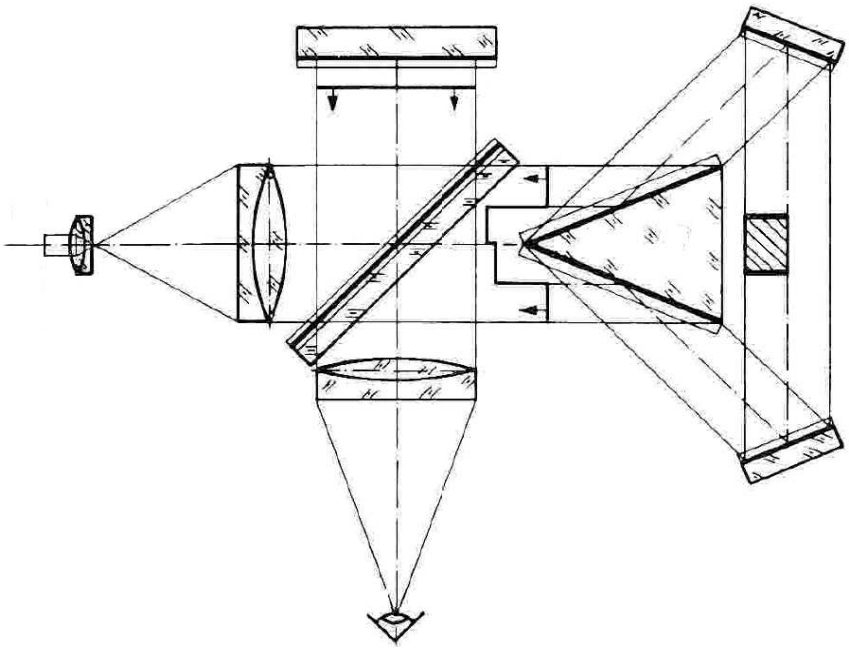

Figure 2.9 Schematic diagram of the Dorenwendt interferometer, source [13].

This work, performed at PTB, is basically motivated by the assumed need to characterize a so called “wringing film” whose thickness should be measured by comparison with the length obtained in the conventional design. Such wringing film thickness was later found to be negligible compared to other effects related to wringing inherent in most of the practical applications of GB length measurements by interferometry. For this reason, the idea of DEI was put aside at PTB until recent years.

2.4.4 Ring Interferometer

In 1983, Khavinson proposed a ring optical scheme as an alternative measurement method for measuring the absolute length of the GBs [14].

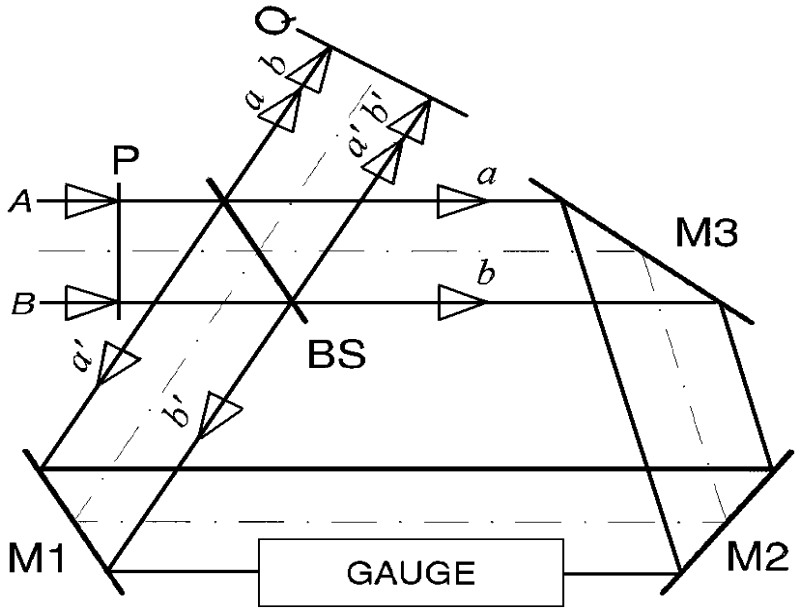

Figure 2.10 Schematic diagram of the ring interferometer, source: [15].

Later Khavinson reported a variety of means to control the optical phase differences in this interferometer [15].

2.4.5 NPL Interferometer

In 1993 Lewis reported the set-up of a DEI at NPL which was part of NPL's Primary Length Bar Interferometer [4]. To measure GBs without platen, the design requires one additional pair of mirrors which are used in the form of a pair of roof mirrors as shown in Figure 2.11.

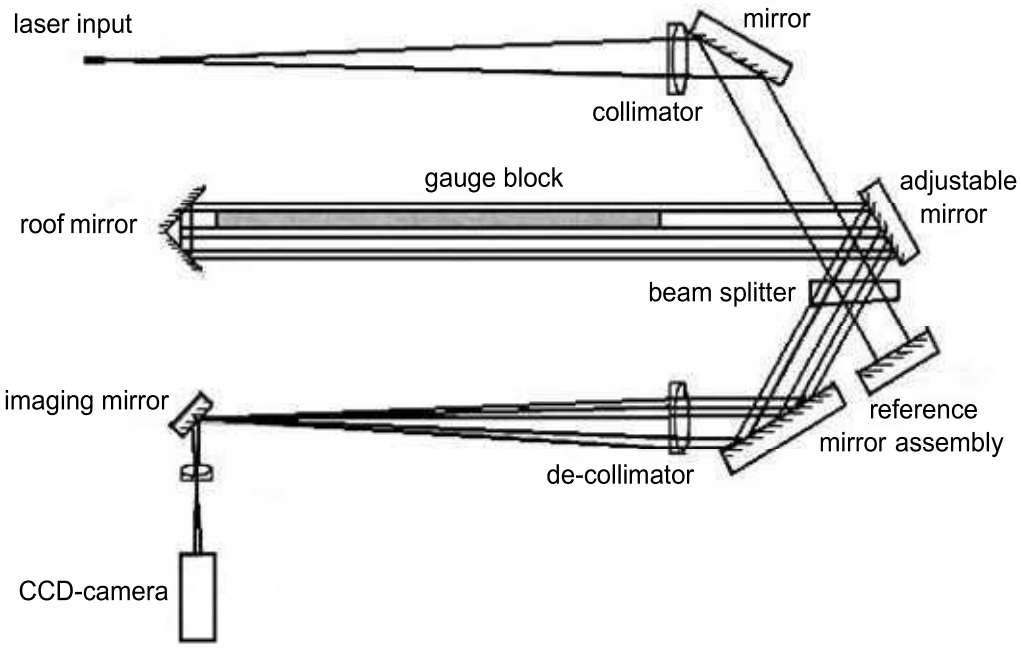

Figure 2.11 Schematic diagram of the NPL interferometer, source: [4].

2.4.6 Other Double-Ended Designs

Similar designs have been suggested by 1998 [16] and 2003 [17].

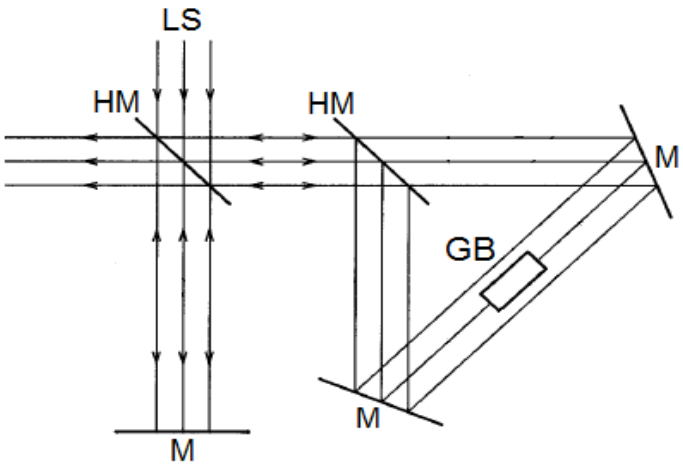

Figure 2.12 Schematic diagram of a DEI, source: [16].

2.4.7 Mitutoyo Interferometer

The technical progress in GB interferometers was combined with the idea of a double-ended design by Kuriyama in 2006 [18] building the first DEI which was equipped with CCD-cameras and phase stepping interferometry. This interferometer was situated in a laboratory of a GB manufacturer company (Mitutoyo Co., Japan) and was built mainly for the purpose of quality control of the production process of GBs [19].

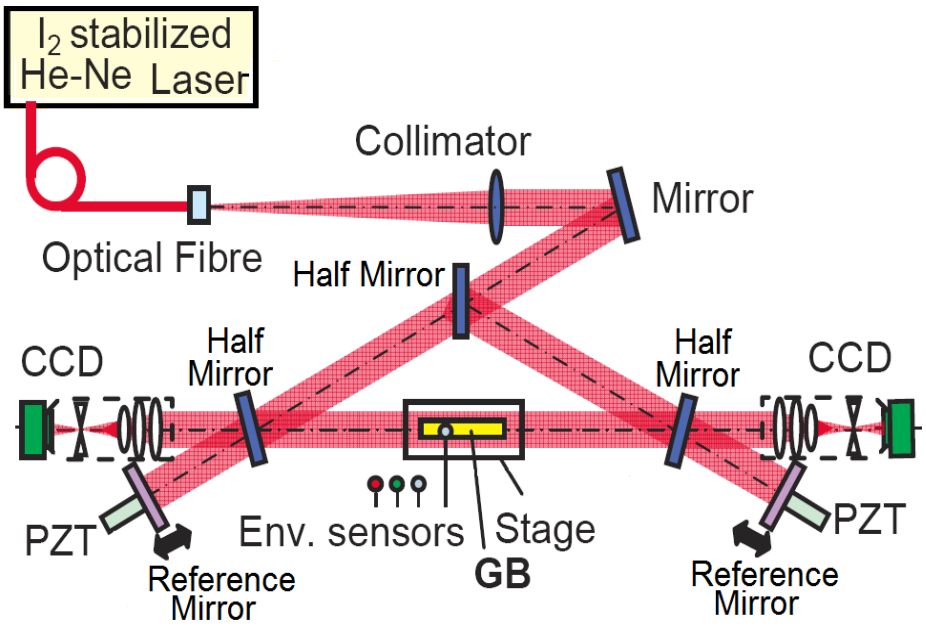

Figure 2.13 Schematic diagram of the Mitutoyo interferometer, source: [18].

Due to the high technology and less numbers of the optical components used in this interferometer, this design can be considered as the best one to measure the GB length when using more than one wavelength. The work of this thesis presents a prototype version of DEI at PTB. This PTB-DEI is similar to the Mitutoyo interferometer that is reported in [18]. However, more than one wavelength is used which makes this interferometer much more effective for

the accurate extraction of the integer orders of interference. A special design for the light source had to be found to allow for the same adjustment states at the different wavelengths.

2.5 Phase Correction

Corrections must be applied to the length measured in the DEI to take account of the phase change on reflection at the surfaces of the GBs and their roughness. This correction is larger than when the GB is wrung to a platen, since in case of the DEI, the effects of phase change on reflection and surface roughness lead to additives from both sides of a GB. This is different in the SEI in which the GB is wrung to a platen and only the difference between the corrections for the two surfaces is effective. This difference ought to cancel out since the GB and the platen should have similar surface properties. The corrections for the surface roughness and the phase change on reflection are often combined into a single correction termed as “phase correction” [4].

2.5.1 Phase Change on Reflection

When light is reflected at normal incidence off the surface of a non-dielectric material, there is a phase change somewhat less than π radians, depending on the optical properties of the media. This is the case when the beam in the interferometer reflects off the surfaces of the GB. For light travelling in air, the phase change on reflection is given as [20]:

$$\delta = ArcTan\left[\frac{2\kappa}{1-n^2-\kappa^2}\right], \tag{2.3}$$

where κ is the extinction coefficient in the reflecting medium and n the refractive index of the reflective medium.

Typical length equivalent values for the phase change on reflection of steel, which are obtained by multiplying half of the wavelength, are summarized in table 2.1.

Wavelength/nm	n	κ	$\frac{\lambda}{2}\delta$/**nm**
532	1.9	3.2	-19.56
633	2.2	3.4	-20.94

Table 2.1 Typical values for n, κ and for the corresponding length equivalent phase on reflection found for steel, see e.g. [21-23].

Therefore, in the DEI, the incident light on the both sides of the GB appears to be reflected approximately 20 nm inside each end surface, even if the surface is perfectly smooth.

2.5.2 Surface Roughness

At PTB, the surface roughness for each individual surface of a GB ends is determined by using an integrating sphere as described in [24]. In this technique, see Figure 2.14, the roughness of the test surface is proportional to the square root of the ratio between the diffused light and the reflected light of the GB surface.

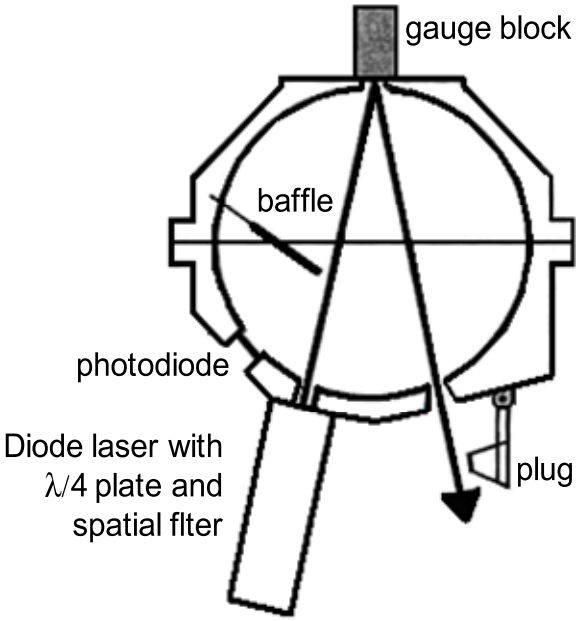

Figure 2.14 Schematic diagram for the integrating sphere, source: [24].

After applying the phase correction to the measured length, the comparison between the definitions of the mechanical length and the corrected optical length shows that the mechanical one is larger as shown in Figure 2.15.

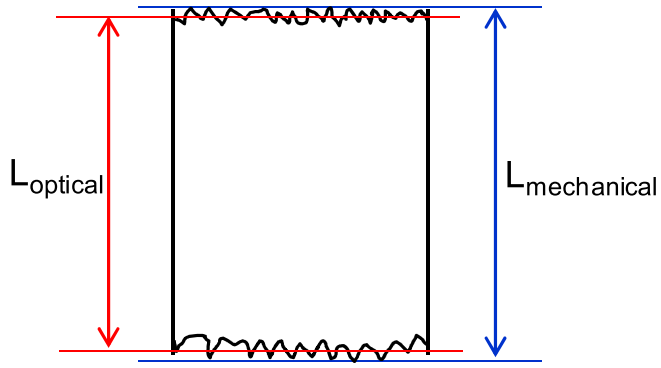

Figure 2.15 Difference between the definition of the length measured optically, after adding the phase correction, and that measured mechanically for the same GB.

Chapter 3

The Design of the Interferometer

In the following, the design of the DEI is presented. The two frequency stabilized lasers, fibers, optical components, and the computer system which controls the entire measurement procedure are described.

3.1 Optical Design of the Interferometer

3.1.1 Description of the Interferometer

A schematic diagram of the experimental setup is shown in Figure 3.1. The optical table of the interferometer is a Newport Scientific series, 1.5 m×3.6 m and the overall size of the interferometer is approximately 1.3 m×2.4 m×0.25 m with beam diameter of 0.06 m.

The light sources for the interferometer are two iodine-stabilized lasers (see § 3.2.1) a Neodymium doped diode (Nd)-Yttrium Aluminium Garnet (YAG) laser at 532 nm (green) and a Helium-Neon (He-Ne) laser at 633 nm (red) connected to a beam combiner equipped with two built-in shutters to switch between them.

The light is led to the interferometer by a single mode fiber connected to the beam combiner and diverges with an angular spread that is dependent on the numerical aperture of the fiber, 0.13.

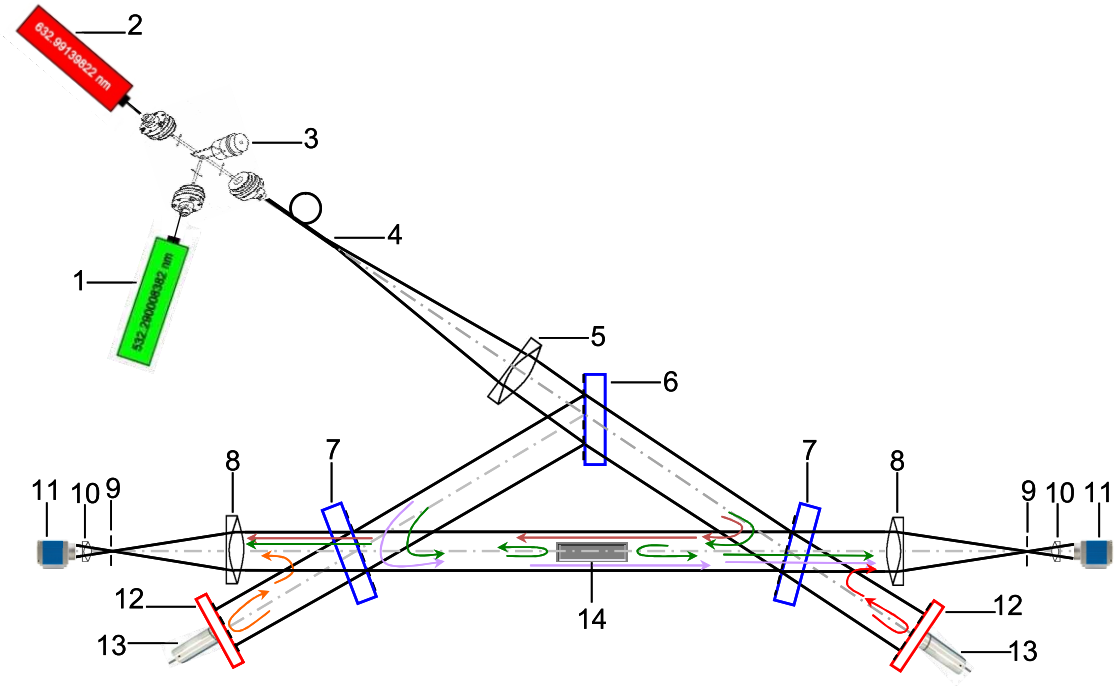

Figure 3.1 Scheme of PTB's prototype DEI. 1- frequency-doubled Nd:YAG laser, iodine-stabilized, 2- He-Ne laser, iodine-stabilized, 3- beam combiner with shutters, 4- single mode fiber output, 5- beam collimator, 6, 7- metal coated beam splitter plates, 8- achromatic lenses, 9- output apertures, 10- output collimators, 11- CCD-cameras, 12- reference mirrors, 13- piezo actuators, 14- GB.

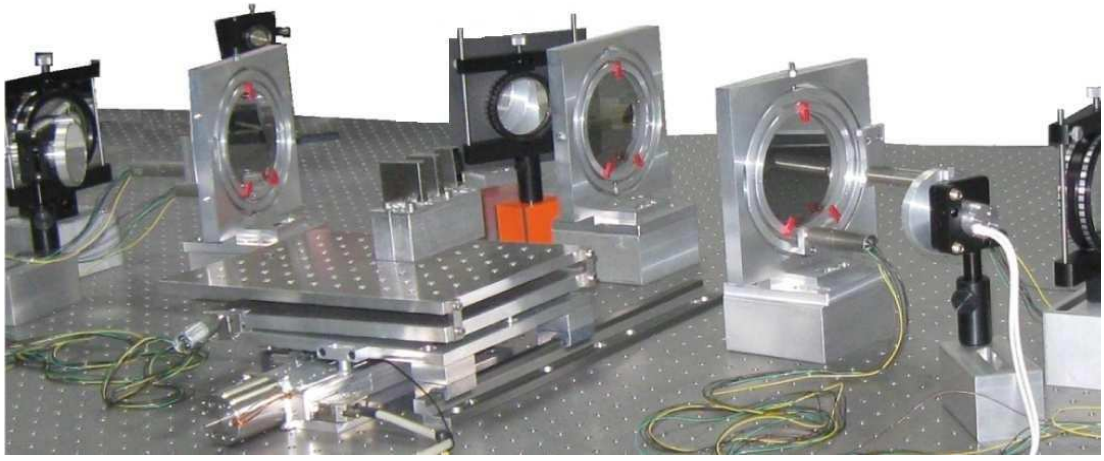

Figure 3.2 Photograph of the DEI prototype built on the tabletop (without enclosure).

After the beam is collimated, it is sent into a triangular shaped interferometer arrangement comprising three beam splitters plates (100 mm diameter). The laser beam passing through the first beam splitter is split into two beams, one to the second beam splitter and the other to the third beam splitter. Then each beam is split into two beams.

When the interferometer is empty i.e., without GB, one part of the divided beam of the second and third beam splitter goes to the reference mirror and the other goes to the other beam splitter. The reference beam is reflected from the reference mirrors, whereas the measurement beam is reflected from the other beam splitter. While when GB is present, the measurement beam is reflected not only from the other beam splitter but also from the GB face. These reflected beams are then combined by passing through the imaging system consisting of the output collimator and an additional lens in front of each CCD-camera which detects the interference as shown in Figure 3.3.

(a) (b)

Figure 3.3 Interference pattern of the DEI when the GB is (a) absent and (b) present.

3.1.2 The Interferometer Chamber

The setup (except the camera and lasers) is housed within a rubber-walled chamber to reduce the effects of air fluctuation, air temperature change and radiated heat from equipments. This is because the accuracy of the interferometer is dependent on knowing accurately the refractive index of the air in the measurement beam and the accurate fringe fraction measurements require stable fringes.

3.2 Interferometer Components

3.2.1 Lasers

Two frequency-stabilized lasers are used in the interferometer, He-Ne/I_2 and Nd:YAG/ I_2. Both lasers are stabilized using saturation absorption with gas cell according to BIPM guides [25, 26]. The two lasers systems are discussed briefly below.

The He-Ne gas laser is based on a medium with a mixture of helium to neon gas in the ratio 8 to 1 with a total pressure of a few millibars. The laser consists of an optical cavity formed by a plasma tube with optical quality mirrors at the ends. The gas in the tube is excited by a high voltage discharge. Then plasma is created in the tube which emits radiation at various wavelengths corresponding to the multitude of allowed transitions in the helium and neon atoms.

The radiation of the He-Ne laser is stabilized with an iodine cell external to the laser, having a cold-finger temperature of 15°C. The absorbing molecule is $^{127}I_2$, and the transition is the a_{16} or f component, R (127) 11-5 at a

frequency of 473,612,353,604 kHz corresponding to a vacuum wavelength of 632. 991 212 58 nm with a relative standard uncertainty of 2.1×10^{-11} [26].

Neodymium doped into YAG crystal is a four-level system. The lower threshold pump power needs four energy levels to achieve a sufficient inversion for a laser operation. A Nd:YAG laser can be pumped using lasers of different wavelengths. Low wavelengths such as 532 nm is produced by frequency doubling of Nd:YAG radiation passing through a non-linear crystal [27].

The radiation of a frequency-doubled Nd:YAG laser is stabilized with an iodine cell external to the laser, having a cold-finger temperature of −15°C. The absorbing molecule is $^{127}I_2$ and the transition is the a_{10} component, R (56) 32-0 at a frequency of 563,260,223,513 kHz corresponding to a vacuum wavelength of 532.245036104 nm with a relative standard uncertainty of 8.9×10^{-12} [27].

3.2.2 Beam Combiner

A beam combiner connected with a fiber end is designed to transmit two separate wavelengths alternatively with best possible transmission (designed by Schäfter + Kirchhoff). The beam combiner is equipped with two built-in electrical shutters at 90 degree to switch between them. This system allows for almost optimum illumination of the interferometer at both wavelengths used.

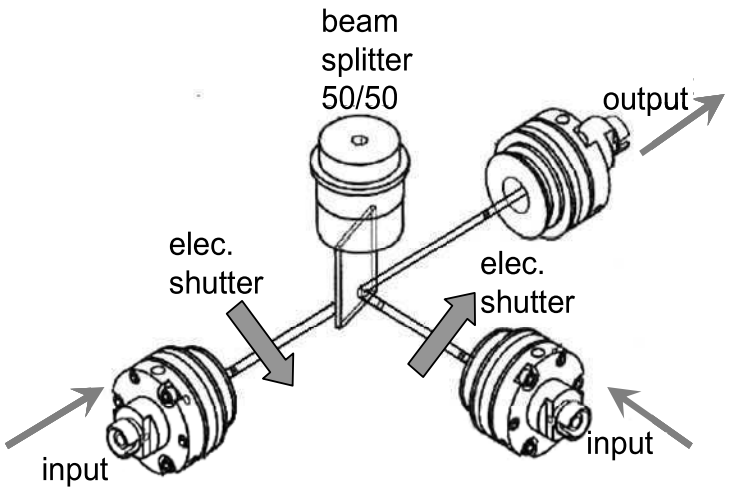

Figure 3.4 Beam combiner together with electric shutters, source: [28].

3.2.3 Laser Attenuator

The Laser attenuator, shown in Figure 3.5, is used for a reproducible and precise laser output power reduction. The Laser intensity is reduced by feeding a precision ball on a micrometer screw into the beam. Mode filtering is performed by a subsequent fiber coupling. A wide range of controlled laser powers (0.5 to > 60 dB) is achievable reproducibly [29].

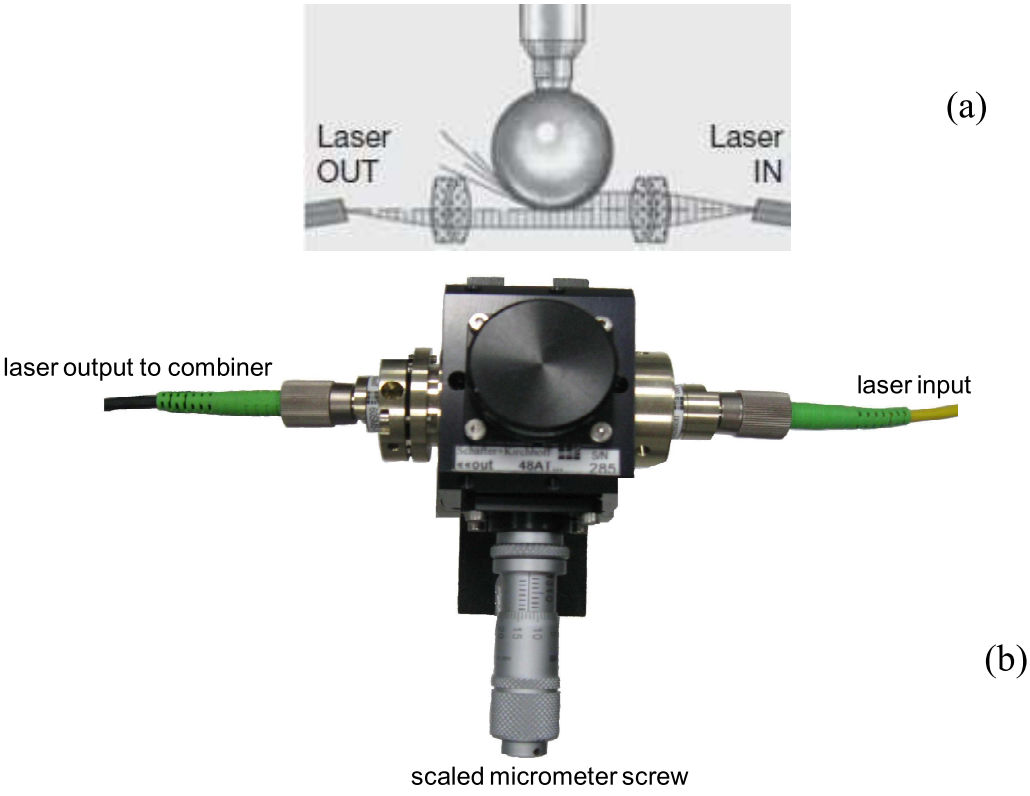

Figure 3.5 (a) Sketch of the working principle of a laser beam attenuator, source: [29]. (b) Used device (48AT, Schäfter + Kirchhoff).

In the DEI, the red laser is not attenuated because its output power is sufficient for the interferometer and imaging of the interference fringes by the CCD-camera. The laser attenuator is only used for the green laser to control the laser power. Lower power is used to protect sensitive cameras from

damage while performing the measurements. The highest power is used only when the autocollimation is tested and at this operation the camera should be closed.

3.2.4 Single Mode Fiber

The interference of the DEI takes part between the normal reference beam and a sheared version of the measurement beam. This requires not only temporal coherence of the doubled path length in SEI, but also spatial coherence across the beam, which is sheared. For this reason a single mode fiber with diameter of 2.8 μm is used as a light source in the focal point of the collimator. The green or the red light enters a short (0.5 m) single mode fiber.

3.2.5 Collimator

The divergent beam from the fiber over-fills the collimator lens (800 mm focal length and diameter 60 mm). This leads to a numerical aperture of 0.04 at the source. From the lens the beam emerges fully collimated due to a positioning of the fiber ends in the focal point of the collimator lens (see Figure 3.1).

When using a collimator of large focal length, the obliquity effect due to the size and positioning error of the source is small (see § 5.3.4).

3.2.6 Beam Splitter Plates

After collimation, the light enters the triangular shaped interferometer arrangement comprising three beam splitter plates (see Figure 3.6). They have flatness better than $\lambda/20$ for good wavefront quality. One side of each plate

has a chrome coating with a 50% transmission prepared by PTB. The other side of the beam splitter plates has an anti-reflection coating (99.9 %) (Fa. Tafelmaier) in order to minimize unwanted reflections and potential parasitic interference effects.

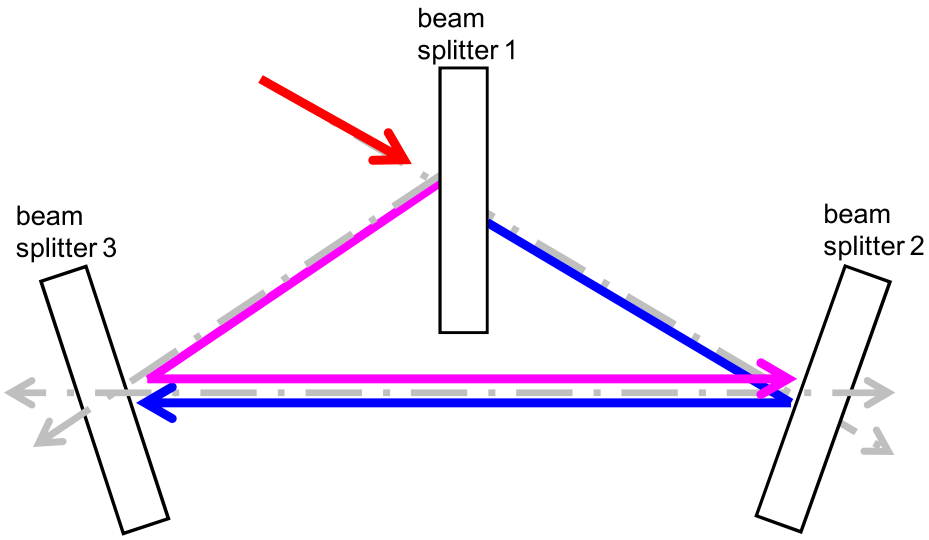

Figure 3.6 The triangular shaped beams paths of the interferometer.

The second and the third beam splitters can be adjusted by motorized micro pusher screws (MICOS) along the horizontal and vertical axis with resolution of 0.2 µm and a maximum displacement of 6 mm, to allow for autocollimation adjustment, as described in § 3.4.

Figure 3.7 A micro pusher connected to the beam splitter, source: [30].

3.2.7 Reference Mirrors

In each arm of the interferometer there exist a reference mirror that reflects the reference beam. The reference mirror (60 mm diameter) is mounted in normal incidence to the beam. Each reference mirror is aligned by a three axes Z/Tip/Tilt piezo actuator system (PI), see Figure 3.1. Such a translator uses piezo-electric translators (PZT) based on solid state ceramics. They convert electrical energy directly to mechanical energy of linear motion [31]. This actuator system is used to establish phase stepping interferometry, PSI, by simultaneously shifting the three axes by exactly the same distance.

The mount of the mirror connected to the table of the interferometer is manufactured by PTB. It has a convenient height to that the collimated beam covers the whole area of the mirror and it can be moved easily in all directions as shown in Figure 3.8.

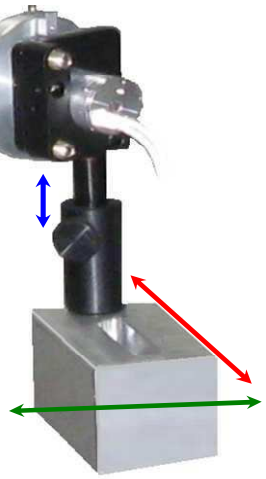

Figure 3.8 Movement directions of the reference mirror mount.

3.2.8 GB Stage

The GB is placed horizontally inside the interferometer between the second and the third beam splitter plates and its length is measured in that position. The dimensions of the table help in measuring short and long GBs. The GB is supported at two points named the airy points as shown in Figure 3.9 [4]. The GBs are moved into the beam by a translation stage and aligned by a self made adjustment unit involving motorized micropushers with resolution of 0.001 mm. (both systems from MICOS), see Figure 3.10.

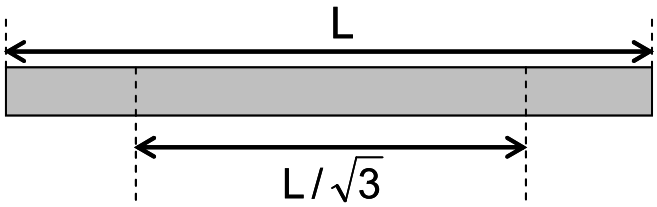

Figure 3.9 The placements of the airy points on the GB, source: [4].

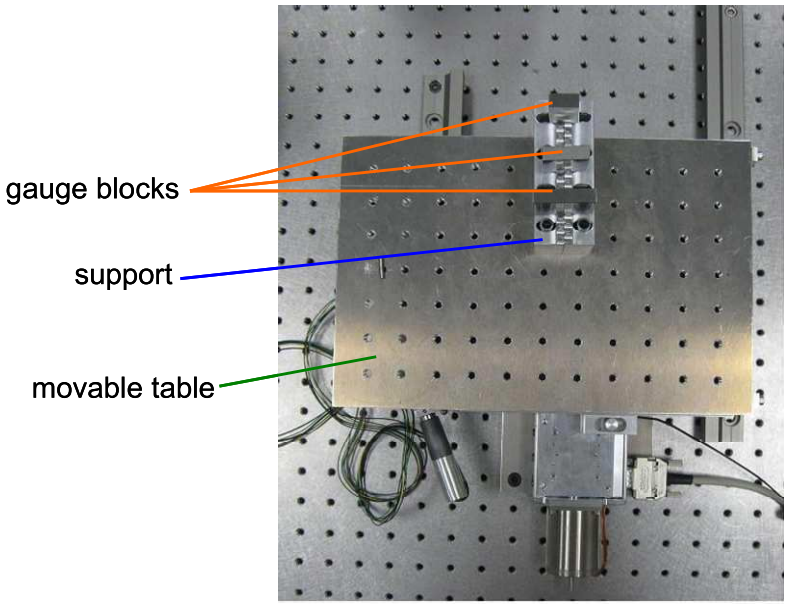

Figure 3.10 GB support attached to a translation (movable) stage.

3.2.9 Imaging Optics and Camera

The two opposite end faces of a GB are each imaged to a CCD-array in both interferometer arms, separately. Each imaging system involves an output collimator L_1 of focal length 500 mm and an additional lens L_2 of focal length 40 mm in front of a 12-bit low noise camera (PixelFly, PCO).

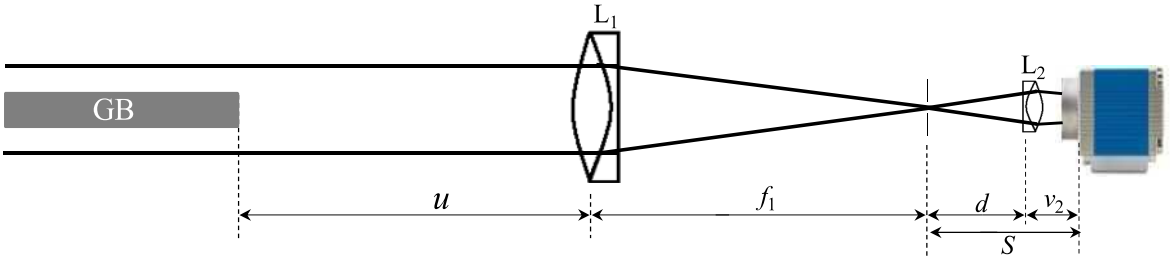

Figure 3.11 The schematic diagram of the imaging system.

For optimum sharpness when handle different GB lengths, the distance between L_2 and the CCD-sensor v_2 must be adapted to the individual position of the end faces of a GB. The distance v_2 can be determined as follow:

From Figure 3.11 the following relation is obtained:

$$f_1 + d = u_2 + v_1, \tag{3.1}$$

and the general lens equation for L_1:

$$\frac{1}{f_1} = \frac{1}{u_1} + \frac{1}{v_1}, \tag{3.2}$$

are used, where f_1 is the focal length of the first lens, d is the distance between the pinhole and the second lens, u_2 is the distance between the image

resulted from the first lens and the second lens, v_1 is the distance between the focal length of the second lens and the image, and u_1 is the distance of the GB face from lens L_1.

By substituting v_1 from equation (3.2) into equation (3.1) and using the law of compound magnification of two lenses *M*:

$$M = \frac{v_1}{u_1} \cdot \frac{v_2}{u_2}, \tag{3.3}$$

hence, the distance v_2 can be written as:

$$v_2 = M \left\{ \left(\frac{d \cdot u_1}{f_1} \right) - d - f_1 \right\}. \tag{3.4}$$

A clear and sharp interference pattern is produced when taking into account the distance v_2 according to equation (3.4). Then the phase values can be calculated accurately.

3.3 SEI Method using the DEI

The length of GB wrung to a platen can be measured using the DEI by closing the path of one arm of the DEI, as shown in Figure 3.12. This provides a useful research tool to the interferometer about the phase correction measurements by comparison of measured lengths of the two different techniques using the same interferometer.

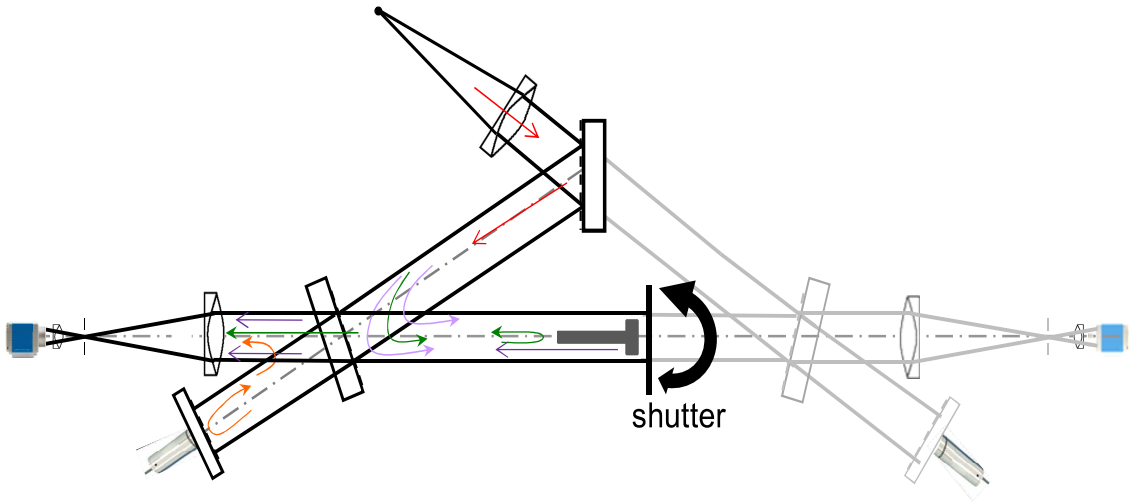

Figure 3.12 Schematic diagram for the DEI when used as SEI.

3.4 Autocollimation Alignment

A cosine error occurs when the direction of the light beam is not normal to the end faces of the GB. In order to achieve perpendicular incidence, the retro-reflected beam of the green laser is observed at the entrance of the interferometer while performing the following steps:

i) the fiber end is positioned to the exact focal point of the collimator. For this purpose a mirror can be placed behind the collimator mount so that the reflected light generates a return spot. The fiber position is then adjusted until the position of the return spot coincides with the position of the fiber end,

ii) after replacement of the mirror, the primary return spots from the interferometer, in the absence of a GB, are observed, while the beam splitter plates are adjusted, until the two return spots coincide with the fiber end as good as visual observation allows. After this procedure, each reference mirror for of each side in the empty interferometer is adjusted while observing the interference pattern. Perpendicular incidence is then achieved when the number of visible fringes is almost zero,

iii) finally the GB is placed and controlled by a movable table and aligned in such a way that minimum numbers of fringes in the interference patterns are achieved for both of the GB's faces.

3.5 Environmental Measurement Parameters

Accurate measurements of air temperature, pressure and humidity are essential if the refractive index of air is to be calculated accurately using empirical equations described in § 4.2.

3.5.1 Temperature measurement

In interferometric length measurements, temperature measurement and stabilization in the interferometric chamber are highly important. Thus, accurate temperatures measurements of the GB at different points along the GB surface and the air around it are required in the DEI.

In the DEI, the temperature is measured by Pt-100 sensors (platinum resistance thermometer) connected to a data acquisition/switch unit (34970A, Agilent). Two sensors are used for surface temperature measurement of the GB and one is used for the air temperature measurement inside the chamber. The GB temperature sensors are integrated into a small copper plate of a clip, which can be clamped to the GB so that good temperature contact is ensured. The air temperature sensor is located near the GB.

The resolution of the temperature readings is 1 mK and the standard measurement uncertainty for the calibration of each sensor is 5 mK. To achieve temperature equilibrium, the GBs were set into the interferometer sufficient time before starting the measurements. The computer records the reading from the temperature sensors in intervals of 10 seconds.

3.5.2 Pressure measurement

The air pressure measurement device should be placed on the same height of the GB. It is measured using a 745-16B Laboratory Barometric Standard (Digiquartz Pressure Instrumentation) with ±8 Pa accuracy [32].

3.5.3 Humidity measurement

Humidity is measured using Testo 650 with a sensor accuracy of ±1 %RH [33].

3.5.4 CO_2 Contents measurement

Because the effect of the CO_2 content on the air refractive index is small (see § 4.2) the value of CO_2 contents in air is taken as 400 ppm with uncertainty of 30 ppm.

3.6 Software

The program has approximately 6000 lines of Visual Basic 6 code (Microsoft). Three PCs are used in the interferometer. One is connected to the three temperature sensors. The other two PCs are connected to one arm of the interferometer, each. On one of these two PCs, the main program of the interferometer is installed which controls the other two PCs using Visual Basic. By using a network between the PCs, the temperature readings can be transferred to the main PC. All commands and steps in both arms can be controlled by the main PC Visual Basic program. The program switches between the used two lasers with a default of starting the measurement with the green laser.

The PZT are controlled by the PCs of the two arms following the installation of software. Therefore the actuator can be moved in definite intervals by giving the step sizes as inputs to the interface of the program.

The program also controls the cameras in both arms of the DEI. Each camera captures a set of phase shifted interferograms recorded at five defined z-positions of the reference mirror.

The coordinate system of the image processing is shown in Figure 3.13 [34]. The axes are marked with x and y, the coordinate pairs correspond to pixels of the camera array. The pixel numbering begins with "0" and ends with "511", yielding a 512×512 pixel camera result.

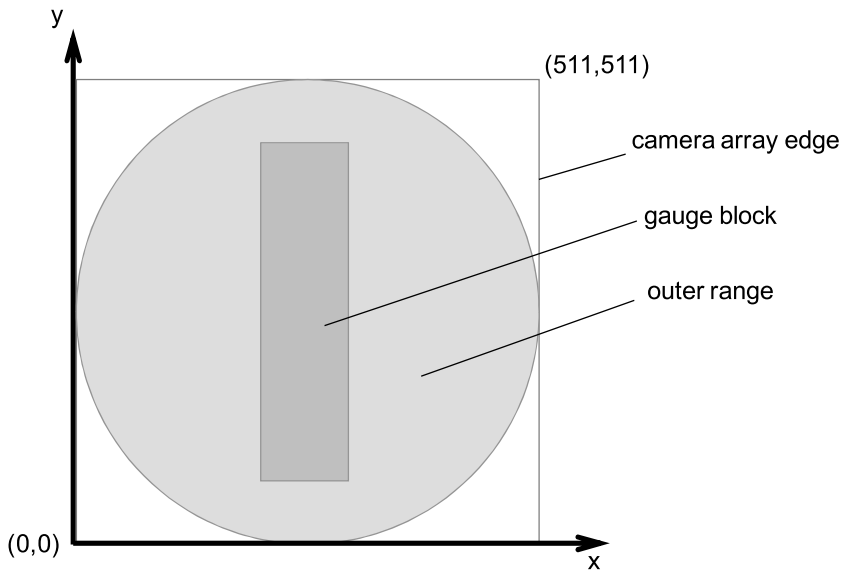

Figure 3.13 The coordinate system of the phase map, source [34].

From the stored data of the five images, the phase at any point in the image can be computed and a phase map of the whole image is built up. Phase shifts between the GB and the reference mirror can be determined. From the phase map of each arm, the program can calculate the fractional of the interference order.

The refractive indices of air at the two measurement wavelengths are calculated using the modified Edlén equation from the measurements of pressure, temperature, humidity and CO_2 content by the software.

Finally, the program applies the exact fractions method (see § 4.3) and finds the coincident values of both wavelengths. Then the average measured length of the GB can be determined. All the measurement data can be saved and then recalled.

Chapter 4

Measurement Method and Data Processing

In the following it is discussed how the DEI can be used to measure the GB length of theoretically and experimentally. The data analysis and information processing are presented.

4.1 DEI Length Measurements Principle

In the DEI, the length of a GB, l_{GB} , can be extracted by considering the relevant pathways of light as depicted in Figure 4.1.

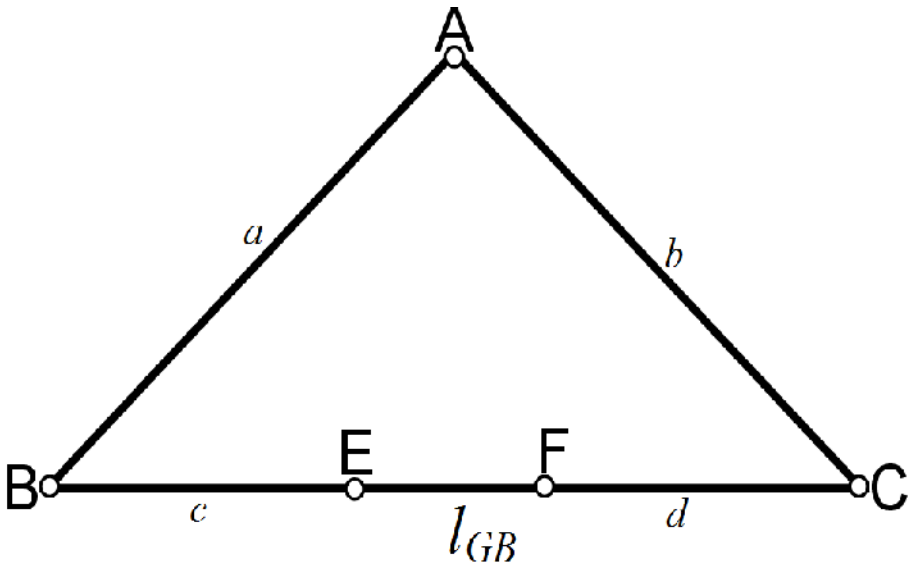

Figure 4.1 The geometrical distances within the DEI ($a = \overline{\mathrm{AB}}$, $b = \overline{\mathrm{AC}}$, $c = \overline{\mathrm{BE}}$, $d = \overline{\mathrm{FC}}$, $l_{GB} = \overline{\mathrm{EF}}$).

The following pathways are related to the measured interferograms and can be expressed in units of the wavelength:

$$l_{(1)} = a + c + l_{GB} + d = \lambda_k \left(N_{(1)} + \tfrac{1}{2\pi} \phi_{ra} \right) \tag{4.1a}$$

$$l_{(2)} = b + 2d \qquad = \lambda_k \left(N_{(2)} + \tfrac{1}{2\pi} \phi_{ra}^{GB} \right) \tag{4.1b}$$

$$l_{(3)} = b + d + l_{GB} + \mathrm{c} = \lambda_k \left(N_{(3)} + \tfrac{1}{2\pi} \phi_{la} \right) \tag{4.1c}$$

$$l_{(4)} = a + 2\mathrm{c} \qquad = \lambda_k \left(N_{(4)} + \tfrac{1}{2\pi} \phi_{la}^{GB} \right), \tag{4.1d}$$

in which $N_{(1)}$ to $N_{(4)}$ are integer orders, λ_k is the wavelength of the used light, and ϕ indicate averaged unwrapped phase values (see § 4.4.2) of the indices ra (right arm), GB (gauge block), and la (left arm). According to Figure 4.1 and equation (4.1), the length of a GB is:

$$l_{GB} = \frac{1}{2} \left(l_{(1)} - l_{(2)} + l_{(3)} - l_{(4)} \right). \tag{4.2}$$

Consequently, the length can be written as:

$$l_{GB} = \frac{\lambda_k}{2} \left\{ i_k + \overbrace{\underbrace{\tfrac{1}{2\pi} \left(\phi_{ra} - \phi_{ra}^{GB} \right)}_{q_k^{ra}} + \underbrace{\tfrac{1}{2\pi} \left(\phi_{la} - \phi_{la}^{GB} \right)}_{q_k^{la}}}^{q_k} \right\}, \tag{4.3}$$

in which i_k is the integer order and q_k is the fractional order of interference. The latter is written as a sum of fractional orders obtained from interferogram analysis in the right and the left arm, respectively, of the DEI (q_k^{ra} and q_k^{la} as indicated in equation (4.3)).

Thus, the length measurement principle of the DEI is the same as the principle described in § 2.1, i.e. the equation of the length to be measured is expressed as:

$$l_k = \frac{\lambda_k}{2} (i_k + q_k) \qquad k = 1 \, , \, 2 \, . \tag{4.4}$$

The next sections of this chapter will describe how each parameter of equation (4.4) can be determined experimentally.

4.2 Determination of the Refractive Index of Air

The wavelength in air λ_k results from the vacuum wavelength, λ_o, scaled down by the amount of the refractive index of air:

$$\lambda_k = \lambda_o / n_k \,. \tag{4.5}$$

For the highest precision of interferometric length measurements in air, n_k can be determined using two main methods. The first one is the modified Edlèn's formula based on simultaneously measured air parameters such as temperature, pressure, humidity and CO_2 content [35-38]. The second method is the use of refractometers with a vacuum cell and the refractive index is measured by using the passed interference fringes when filling or evacuating the vacuum cell [39].

The calculation of n_k using the modified Edlèn's formula [36] starts with the dispersion formula of dry air for input parameters: temperature 20 °C, pressure 10^5 Pa, relative humidity 50 %, and 0.04 % CO_2 content describing the refractivity of air dependent on the vacuum wavenumber σ in μm^{-1} :

$$(n-1)10^8 = \left(8091.37 + \frac{2333983}{130-\sigma^2} + \frac{15518}{38.9-\sigma^2}\right). \tag{4.6}$$

A CO_2 content x, differing from 0.04 %, changes the refractivity to:

$$(n_x - 1) = (n-1)\left(1 + 0.5327\,(x - 0.0004)\right). \tag{4.7}$$

The deviation of temperature t and pressure p is taken into account by:

$$\left(n_{tp}-1\right)=\left(n_{x}-1\right)\left(\frac{p}{93214.60}\right)\left(\frac{1+10^{-8}\left(0.5953-0.009876t\right)p}{1+0.0036610t}\right), \qquad (4.8)$$

where n_{tp} is the refractive index of air, at pressure p in Pascals and temperature t in degrees Celsius.

In the last step the influence of water vapour with partial pressure f is calculated which results in the refractive index n_{tpf} for moist air under total pressure p and for temperature t and CO_2 content x:

$$\left(n_{tpf}-n_{tp}\right)10^{8}=-f\left(0.038020-0.000384\sigma^{2}\right), \qquad (4.9)$$

where n_{tpf} is the refractive index of moist air, and f is the vapour partial pressure of water in Pascals. The vapour partial pressure f is related by definition to the saturation vapour pressure f_s and the relative humidity by R = (f / f_s) × 100, where R is the relative humidity in percent. For the transformation of dew point temperature to water vapour pressure, the equation for the saturation pressure of water f_s given by Giacomo [37] with the updated constants of Davis [38] has been used:

$$f_{s}=\exp\left(AT^{2}+BT+C+DT^{-1}\right), \qquad (4.10)$$

with:

$A=1.2378847\times10^{-5}\ \mathrm{K}^{-2}$, $B=-1.9121316\times10^{-2}\ \mathrm{K}^{-1}$,

$C=33.93711047$, $D=-6.3431645\times10^{3}\ \mathrm{K}$.

Collecting these equations together gives the following empirical equation of the refractive index of air used in the DEI:

$$(n_{tpf}-1)10^8 = \left(8091.37 + \frac{2333983}{130-\sigma^2} + \frac{15518}{38.9-\sigma^2}\right) \cdot \left(\frac{p}{93214.60}\right)\left(\frac{1+10^{-8}(0.5953-0.009876t)p}{1+0.0036610t}\right) - f\,(0.038020 - 0.000384\sigma^2). \quad (4.11)$$

Table 4.1 summarises the effects of the air temperature, pressure, water vapour content (humidity) and CO_2 content on the air refractive index. The air pressure and temperature have the largest effect on the refractive index of air, so accurate measurements of these parameters are essential if the refractive index is to be calculated accurately using the modified Edlén's equations.

Parameter	**Increment**	**Relative Sensitivity**
temperature	1 °C	-9.20×10^{-07}
pressure	1 Pa	$+2.70\times10^{-09}$
CO_2 content	1 ppm	$+1.44\times10^{-10}$
dew point	1 °C	-2.98×10^{-08}

Table 4.1 Effect of environmental parameters on refractivity at standard conditions.

4.3 Determination of the Integer Order of Interference

The large number of the integer order of interference, i_k, can be determined from using more than one wavelength as light source and applying the method of exact fractions [22, 40]. In this technique, variation numbers, δ, are added to estimate integer orders obtained from $i_k = l^{est} / \frac{\lambda_k}{2}$, in which l^{est} is the estimated length. Application of two wavelengths, as in the DEI, results in the lengths: $l_1 = \frac{1}{2}\lambda_1\left(i_1^{est} + \delta_1 + q_1\right)$ and $l_2 = \frac{1}{2}\lambda_2\left(i_2^{est} + \delta_2 + q_2\right)$. Applying a set of δ and detecting the best coincidence between l_1 and l_2 in principle indicates the correct integer order of interference for both wavelengths.

4.4 Determination of the Fractional Order of Interference

From equation.(4.3), the fractional order of interference can be written as:

$$q_k = q_k^{ra} + q_k^{la} = \tfrac{1}{2\pi}\left(\phi_{ra} - \phi_{ra}^{GB}\right) + \tfrac{1}{2\pi}\left(\phi_{la} - \phi_{la}^{GB}\right), \tag{4.12}$$

where the averaged unwrapped phase value ϕ with indices ra (right arm), GB (gauge block), and la (left arm) will be calculated in the next sections.

In phase measurement interferometry, first a phase change is induced between the measured and reference beams, and the interferograms are captured. Then the wavefront phase is calculated from changes in the recorded intensity data. The phase can be shifted by tilting an optical plate, moving a grating, rotating a half wave plate or analyzer and using an acousto-optic or electro-optic modulator.

Phase stepping interferometry, PSI, is used in the DEI to measure the fractions. In this technique, the phase of reference beam is shifted by moving the reference mirror for five steps with respect to the measured beam. Thus, the phase is changed due to the phase difference between the two beams. An image of the fringes is captured by the CCD-camera at each step to determine the phase of each pixel in the image of the interference fringes. As a result, totally 10 images are obtained for each laser wavelength.

4.4.1 Phase Extraction

The intensity of a fringe pattern at a pixel positioned at point (x, y) can be expressed as:

$$I_k(x,y) = a(x,y) + b(x,y)\cos\left[\phi(x,y) + \phi_k\right], \tag{4.13}$$

where $a(x,y)$ is the variation of background intensity, $b(x,y)$ is the modulation of the fringes, $\phi(x,y)$ is the phase to be measured and ϕ_k is the k–th phase shift positions. By omitting (x,y) for convenience and assuming a constant phase shift between interferograms, equation (4.13) can be rewritten as:

$$I_k(x,y) = a + b\cos\left[\phi + (k-3)\alpha\right]. \tag{4.14}$$

The five intensity measurements at a single point in the interferograms are recorded at five defined z-positions of the reference mirror when: $\{k=1:-2\alpha,\ k=2:-1\alpha,\ k=3:0\alpha,\ k=4:1\alpha,\ k=5:2\alpha\}$, in which α is the step width.

The corresponding phase maps are calculated by applying the algorithm introduced by Tang [41]:

$$\tan\phi = \frac{\sqrt{[2(I_4 - I_2) + (I_5 - I_1)][2(I_4 - I_2) - (I_5 - I_1)]}}{I_1 + I_5 - 2I_3}, \tag{4.15}$$

in which I_1 to I_5 are the intensities of the respective interferograms at $k = 1, 2, 3, 4, 5$ at a certain pixel position of the camera.

Figure 4.2 shows examples of a set of interferograms recorded in one arm of the interferometer and the resulting phase maps.

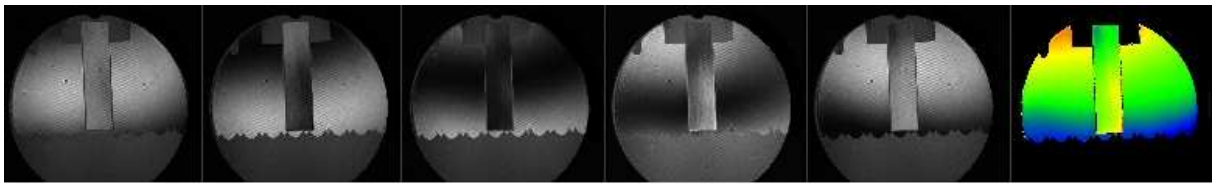

Figure 4.2 Example of five interferograms and the resulting phase map in the right arm of the DEI for a 30 mm ceramic GB sample using the iodine stabilized He-Ne laser.

After phase extraction, the GB position is identified within the interferogram in order to define three regions of interest (ROIs) from a phase map of each arm [42]. They are indicated as black squares in Figure 4.3. The central ROI is set to the position of the front face of the GB while the two others ROIs are arranged symmetrically around the central ROI. The fractional order of interference bases on average phase values within these well defined ROIs.

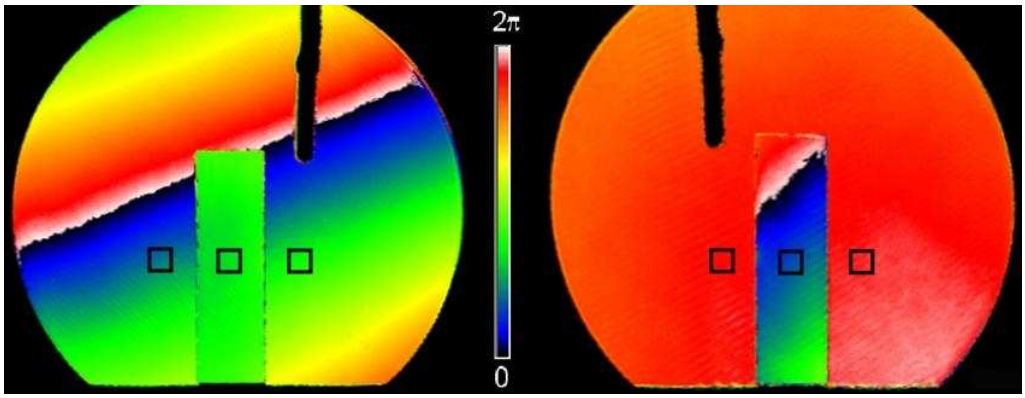

Figure 4.3 Phase maps obtained in the left and the right arm for a 7.5 mm steel GB using the iodine stabilized He-Ne laser. Regions of interest (ROIs) are indicated by squares.

4.4.2 Removal of Phase Discontinuity

Before averaging the phase values within the ROI, it is necessary to remove 2π discontinuities at fringe boundaries. This procedure is called unwrapping and can be performed by processing the phase values within each ROI with respect to phase differences $\Delta\phi$ at neighboring pixel positions. If the difference is greater than a certain threshold such as π, then a phase jump (2π discontinuity) is detected. When the sign of $\Delta\phi$ is negative (the phase is increasing), 2π is added, whereas when the sign of $\Delta\phi$ is positive (the phase is decreasing), 2π is subtracted [4]. In Figure 4.4, a phase map image of the wrapped phase is unwrapped by passing through x direction.

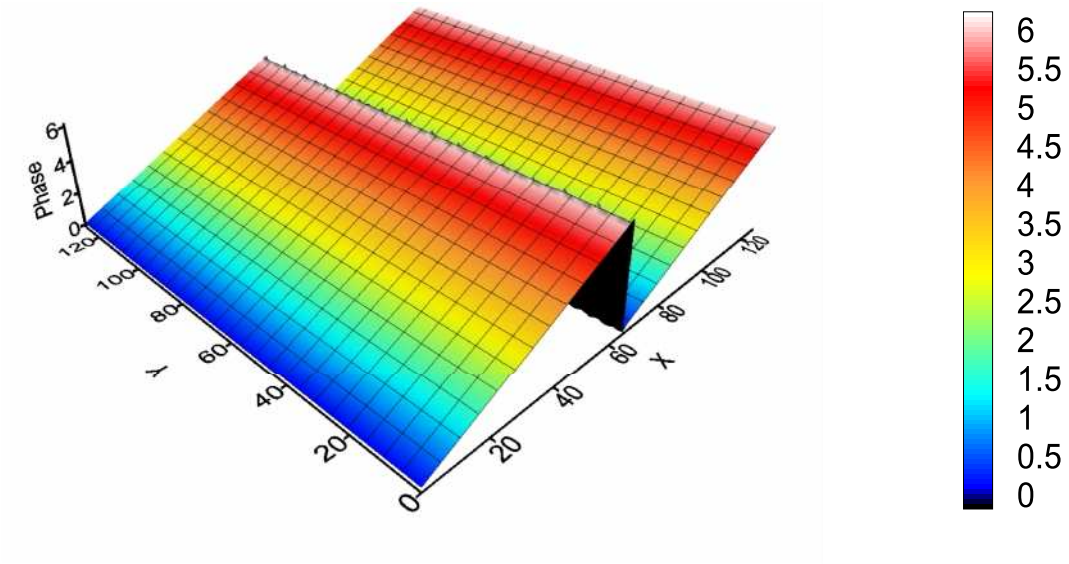

(a)

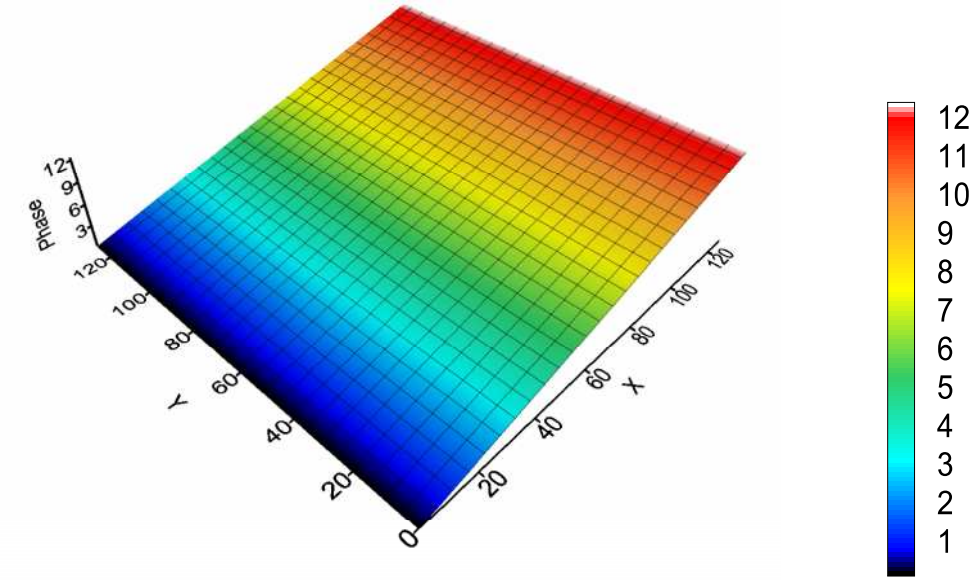

(b)

Figure 4.4 3D simulated phase map profile, (a) wrapping and (b) unwrapping.

Then the averaged phase values are simply obtained [22]:

$$\phi(x,y) = \frac{1}{(x_f - x_i + 1)(y_f - y_i + 1)} \sum_{\substack{x=x_i,\ldots\ldots,x_f \\ y=y_i,\ldots\ldots,y_f}} \phi^{uw}(x,y), \tag{4.16}$$

in which (x_i, y_i) and (x_f, y_f) indicate the initial and final coordinates within each ROI.

Moreover, it is essential that the average phase values of the outer ROIs relates to the same virtual continuous phase topography within the same plane without possible 2π discontinuities by so called “left-right-unwrapping” [22, 42]. This can be obtained by extrapolating the phase taking into account for the slope within the ROIs:

$$\phi_r^{uw} = \phi_r - Round\left[(\phi_l + \phi^x(x_r - x_l) - \phi_r\right], \tag{4.17}$$

in which $x_r - x_l$ is the pixel distance between the ROIs on the left and the right outer sides and ϕ^x the average slope along the x-direction (left to right) detected within ϕ_l and ϕ_r. This evaluation typically gives rise to the addition of a certain integer order of interference to one of the outer ROIs.

Finally, by substituting the resulted average phases in equation (4.12), the value of the fractional order of interference can be determined.

4.5 Corrections

4.5.1 Length Correction to 20°C

Accurate temperature measurements are very essential when length measurements are performed because length measurements are always related to the temperature of the object. In the interferometric calibrations of GBs the quantity to be determined is the length at a reference temperature, 20°C (the ISO standard reference temperature for length measurements) [43]

In the DEI, the length measurement is performed at a temperature t deviating from the reference temperature. For this reason a correction is necessary taken into account the respective temperature deviation. This leads to the length at the reference temperature:

$$L_{20^oC} = L_t \left[1 + \alpha_o \left(20^o C - t\right)\right], \tag{4.18}$$

in which α_o denotes the coefficient of thermal expansion of the GB material. For example, a 1 m GB of steel with a typical thermal expansion coefficient of 1.2×10^{-5} K^{-1} will be measured about 1.2 μm longer at t = 20.100°C than at t = 20.000°C. This illustrates the importance of accurate temperature measurement. Thus depending on the GB's material, the temperature measurements with sub-mk uncertainty may be necessary to obtain the desired uncertainty of the length measurement.

4.5.2 Phase Correction

As mentioned before in § 2.5, the phase change on reflection at the surfaces of the GB and their roughness lead to an additive correction 'phase correction' from both sides of the GB.

4.6 Measured Length of Gauge Block Using the DEI

Using the DEI, the measured length of the GB is set to the average, i.e.:

$$l_{GB} = \tfrac{1}{2}\left(l_1 + l_2\right), \tag{4.19}$$

where l_1 is the measured length using the green laser and l_2 is the measured length using the red laser.

4.7 Measurement Method Steps of a 10 mm Steel Gauge Block using Visual Basic 6

1- In Figure 4.5 the main PC program (see § 3.6) captures five frames of the right arm. In the same time the other five frames of the left arm are captured and recalled from the other PC. The resulted ten frames of the measured GB can be saved.

2- The same step is done for the red laser.

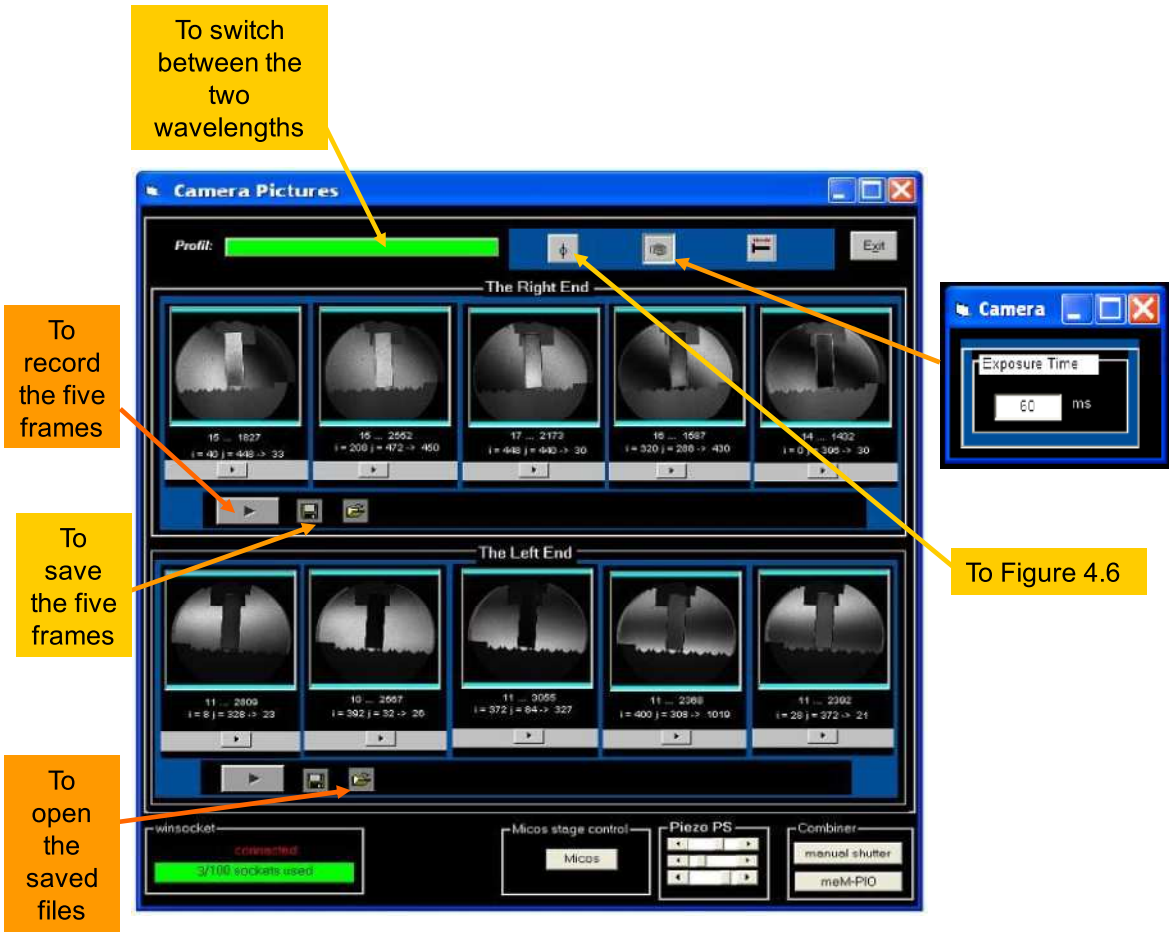

Figure 4.5 The first window in a GB measurement program used in the DEI.

3- The phase map, phase extraction (see § 4.4.1) and removal of phase discontinuity (see § 4.4.2) are shown in Figure 4.6.

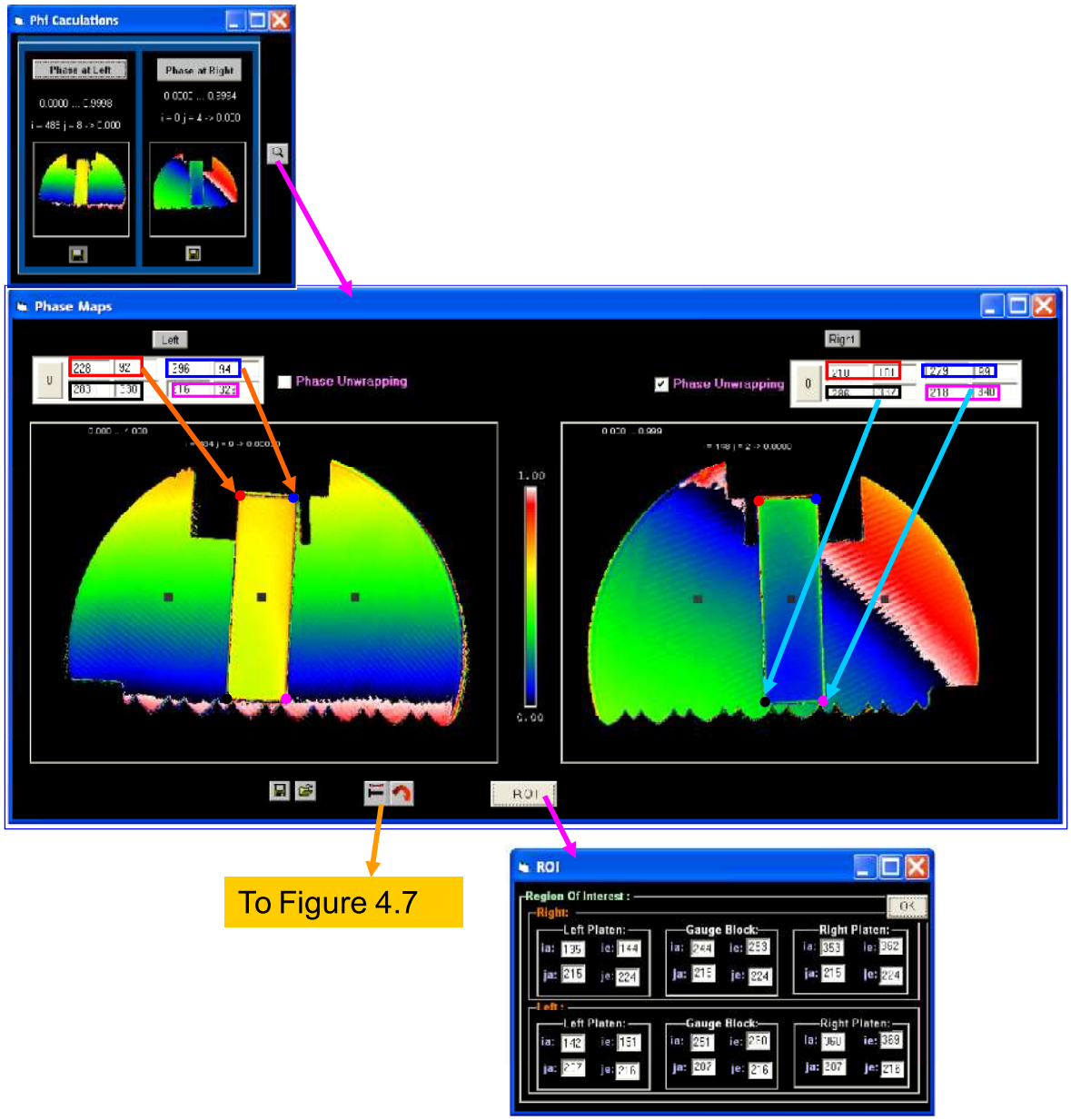

Figure 4.6 The interferogram analysis.

4-The refractive index of air (see § 4.2) and fractions for each wavelength (see § 4.4) are calculated in Figure 4.7.

5- In Figure 4.7, the measured length is determined by taking into account the corrections (see § 4.5) and applying the method of the exact fractions (see § 4.3).

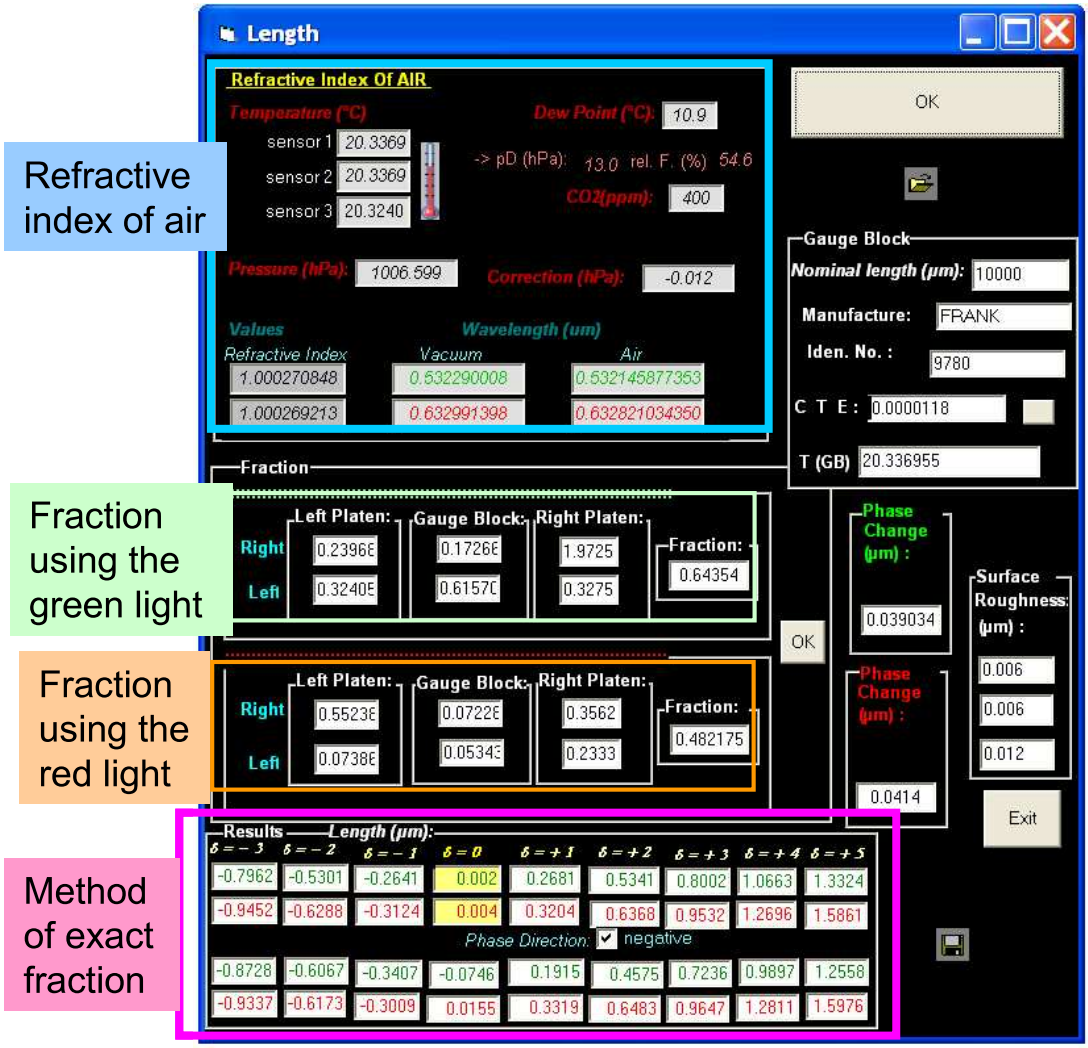

Figure 4.7 The final window of a measurement step.

Chapter 5

Estimation of the Measurement Uncertainty

The uncertainty analysis in a measurement is a fundamental part of metrology. It shows that the accuracy of experimental results should be represented as an addition of uncertainties [34, 44-48].

When GB is measured in the DEI, the result of the length calculation will be subjected to an uncertainty due to the design and operation of the set-up. The total uncertainty will be the sum of many contributing uncertainties.

The estimation of the measurement uncertainty for the DEI is done according to the Guide to the Expression of Uncertainty in Measurement, (GUM) [44], in addition to Ref. [47] which is used as a basis of DEI uncertainty estimation.

5.1 The Uncertainty Calculations

5.1.1 Combined Uncertainty

Combined standard uncertainty $u_c(d)$ is a quadrature sum of the uncertainties $u(x_i)$ of all of the influencing factors x_i , each weighted by a sensitivity coefficient c_i :

$$u_c^2(d) = \sum_{i=1}^{N} c_i^2 u^2(x_i), \tag{5.1}$$

where d is the deviation from nominal length of the GB, $u(x_i)$ are the standard uncertainties attributed to the influencing quantities x_i and c_i is the sensitivity coefficient, represented as:

$$c_i = \frac{\partial d}{\partial x_i}. \tag{5.2}$$

5.1.2 Expanded Uncertainty

Expanded uncertainty $U = k\ u_c(d)$ is defined as the combined standard uncertainty multiplied by a coverage factor k. The main principle is to choose the approximate level of confidence that is relevant to the uncertainties. Generally, measurement values are expressed with a coverage factor of value between 2 and 3.

5.2 Model Equation

For interferometric measurement of a GB, it is convenient to arrange a model equation such that the influencing parameters are kept isolated as much as possible. The GUM technique can then be applied to each of these influencing parameters.

The measured deviation d from the GB nominal length L is:

$$d = l - L, \tag{5.3}$$

where l is the measured length of the GB. The following model equation is suitable for presenting the uncertainty evaluation of the DEI:

$$d = l_{fit} - L + l_t + l_A + l_\Omega + l_v + l_\phi, \tag{5.4}$$

where l_{fit} is the best fit solution for the length of GB for m wavelengths of light and it is expressed by applying the method of the exact fractions as:

$$l_{fit} = \frac{1}{m}\sum_{k=1}^{m}(i_k + q_k)\frac{\lambda_{k(vac.)}}{2n_k}. \tag{5.5}$$

l_t is the GB temperature correction:

$$l_t = \alpha L\,\Delta t, \tag{5.6}$$

where α is the thermal expansion coefficient, $\Delta t = 20^oC - t$, t the GB temperature in degrees Celsius.

l_A is the correction for optics errors, as a result of imperfect interferometer optics.

l_Ω is the correction of obliquity effect due to the size of light source and focal length of the collimator:

$$\begin{aligned} l_\Omega &= \Omega L \\ &= \left(\frac{a^2}{16f^2}\right)L, \end{aligned} \tag{5.7}$$

where a is the aperture diameter and f is the focal length of the collimating lens.

l_v is the correction of GB geometry accounts for non-parallelism and non-flatness of the GB.

l_ϕ is the length equivalent correction for phase change on reflection and surface roughness.

5.3 DEI Uncertainty Evaluations

Applying equations (5.1) to (5.4) yields the combined standard uncertainty in d in terms of the measured quantities and corrections:

$$u_c^2(d) = c_{l_{fit}}^2\, u_c^2(l_{fit}) + c_{l_t}^2\, u^2(l_t) + c_{l_A}^2\, u^2(l_A) + c_{l_\Omega}^2\, u_c^2(l_\Omega) + c_{l_\nu}^2\, u^2(l_\nu) + c_{l_\phi}^2\, u_c^2(l_\phi), \tag{5.8}$$

where each contribution is described in detail below.

5.3.1 Uncertainty Evaluation of l_{fit}

Length uncertainty evaluation based on the method of exact fractions consists of the uncertainties of the integer number of interference order, fringe fraction measurements, sources vacuum wavelengths, and refractive indices:

$$u_c^2(l_{fit}) = c_i^2\, u^2(i_k) + c_q^2\, u^2(q_k) + c_{\lambda(vac.)}^2\, u^2(\lambda_{k(vac.)}) + c_n^2\, u_c^2(n_k)$$
$$= \left(\frac{\partial l_{fit}}{\partial i_k}\right)^2 u^2(i_k) + \left(\frac{\partial l_{fit}}{\partial q_k}\right)^2 u^2(q_k) + \left(\frac{\partial l_{fit}}{\partial \lambda_{k(vac.)}}\right)^2 u^2(\lambda_{k(vac.)}) + \left(\frac{\partial l_{fit}}{\partial n_k}\right)^2 u_c^2(n_k), \tag{5.9}$$

where i is an integer count of interference orders for the GB. Thus $u(i_k)$ is taken as zero.

The combined standard uncertainty can be evaluated by taking the partial derivatives of the equation (5.5):

$$u_c^2(l_{fit}) = \sum_{k=1}^{m}\left(\frac{\lambda_{k(vac)}}{2\,m\cdot n_k}\right)^2 u^2(q_k) + \sum_{k=1}^{m}\left(\frac{i_k + q_k}{2\,m\cdot n_k}\right)^2 u^2(\lambda_{k(vac.)}) + \sum_{k=1}^{m}\left(\frac{i_k + q_k}{2\,m\cdot n_k^2}\right)^2 u_c^2(n_k)\,. \tag{5.10}$$

m is equal 2, since two wavelengths are used. The second term of equation (5.10) can be rewritten by using the relation of $(i_k + q_k)/2m\cdot n_k = L/\lambda_{k(vac.)}$ as:

$$u_c^2(l_{fit}) = \sum_{k=1}^{m}\left(\frac{\lambda_{k(vac.)}}{2m\,n_k}\right)^2 u^2(q_k) + \sum_{k=1}^{m}\left(\frac{L}{m\,\lambda_{k(vac.)}}\right)^2 u^2(\lambda_{k(vac.)}) - \sum_{k=1}^{m}\left(\frac{L}{m\,n_k}\right)^2 u_c^2(n_k)\,, \tag{5.11}$$

Each parameter of equation (5.11) is determined as follows:

- The value of the used vacuum wavelengths and their values and standard uncertainties are given in table (5.1):

Laser Type	VacuumWavelength (nm)	Standard Uncertainty (nm)
Nd-YAG laser	532.290008	$7\times10^{-12}\ \lambda$
He-Ne laser	633.991398	$5\times10^{-11}\ \lambda$

Table 5.1 The laser wavelengths value and their standard uncertainties.

- The refractive index of air can be calculated by substituting the averaged values for a set of DEI measurements of the temperature (t = 20.2 ^{o}C), pressure (p = 100170 Pa), partial vapour pressure (f = 1210 Pa), and vacuum wavelength (table 5.1) in equation (4.11) as 1.00026978 using green laser and 1.000268051 using red laser.

- $u(q_k)$ is determined experimentally and is taken as 0.01 fringe for red laser and 0.008 for the green laser.

- $u(n_k)$, The combined standard uncertainty of refractive index of air is evaluated by taking the partial derivatives of equation (4.11) as :

$$u_c^2(n) = c_t^2 u^2(t) + c_p^2 u^2(p) + c_f^2 u^2(f) + c_\lambda^2 u^2(\lambda) . \qquad (5.12)$$

Before performing measurements, the temperature t, pressure p, wavelength λ, and partial vapour pressure f instruments were calibrated at PTB laboratories. The given standard uncertainties for the instruments of temperature, pressure, humidity and vacuum wavelength are given in table 5.2.

	Value	**Unit**
$u(t)$	0.01	K
$u(p)$	6	Pa
$u(f)$	10	Pa
$u(\lambda)$	2.5×10^{-11}	µm

Table 5.2 The standard uncertainties of the parameters that affect the air refractive index.

The sensitivity coefficients are calculated by partial derivatives of the n_{tpf} in equation (4.11):

$$c_t = \frac{\partial n}{\partial t}, \; c_p = \frac{\partial n}{\partial p}, \; c_f = \frac{\partial n}{\partial f}, \; c_\lambda = \frac{\partial n}{\partial \lambda}. \qquad (5.13)$$

Each of these partial derivatives can be expressed as following:

$$\frac{\partial n}{\partial t}=\left(8091.37+\frac{2333983}{130-\sigma^2}+\frac{15518}{38.9-\sigma^2}\right)\left(\frac{10^{-8}}{93214.60}\right)$$
$$\left(\frac{10^{-8}\left(-0.009876\right)\left(1+0.0036610\ t\right)p^2-0.0036610\left(p+10^{-8}(0.5953-0.009876\ t)p^2\right)}{\left(1+0.0036610\ t\right)^2}\right), \tag{5.14}$$

$$\frac{\partial n}{\partial p}=\left(8091.37+\frac{2333983}{130-\sigma^2}+\frac{15518}{38.9-\sigma^2}\right)$$
$$\left(\frac{10^{8}}{93214.60}\right)\left(\frac{1+2\times10^{-8}\left(0.5953-0.009876t\right)p}{1+0.0036610t}\right), \tag{5.15}$$

$$\frac{\partial n}{\partial f}=10^{-8}\left(-0.038020+0.000384\sigma^2\right), \tag{5.16}$$

$$\frac{\partial n}{\partial \lambda}=\left(\frac{p+10^{-8}(0.5953-0.009876t)p^2}{1+0.0036610t}\right)\left(\frac{10^{-8}}{93214.60}\right)$$
$$\left(\frac{2\times2333983\lambda}{\left(130-\lambda^2\right)^2}+\frac{15518}{\left(38.9-\lambda^2\right)^2}+\left(0.000384\times2\times10^{-8}\,f\,\lambda\right)\right). \tag{5.17}$$

By substituting the averaged values for a set of measurements in equations (5.14), (5.15), (5.16), and (5.17), sensitivity coefficients of refractive index can be calculated and given in table 5.3.

	Senstivity	**Unit**
$\partial n/\partial t$	-4.6×10^{-7}	K^{-1}
$\partial n/\partial p$	2.6×10^{-09}	Pa^{-1}
$\partial n/\partial f$	-3.7×10^{-10}	Pa^{-1}
$\partial n/\partial \lambda$	1.7×10^{-6}	μm^{-1}

Table 5.3 Sensitivity coefficients of refractive index of air.

The combined standard uncertainty attributed to the refractive index calculation is given by using equation (5.12) and making substitutions of the values given in table 5.2 and 5.3 in addition to the uncertainty of the modified Edlén equation at $k = 1$ level of confidence, 1×10^{-8} [47].

$$u_c(n) = 2\times10^{-8}\, L. \tag{5.18}$$

Substituting these values in equation (5.11), then:

$$u_c^2(l_{fit}) = (3.8\ \text{nm}^2) + (1.4\times10^{-8}L)^2\,. \tag{5.19}$$

5.3.2 Uncertainty Evaluation of l_t

The combined uncertainty due to the temperature effects can be found in two parts:

1) part corresponding to the GB temperature measurements,
2) part corresponding to the GB thermal expansion coefficient.

By taking the partial derivatives of l_t, these two components can be found below as:

$$u_c^2(l_t) = u^2(\alpha)\, L^2\, (\Delta t)^2 + \alpha^2\, L^2\, u^2\, (\Delta t), \tag{5.20}$$

where $u(\alpha)$ is the uncertainty of thermal expansion coefficient of the gauge material.

The first term on the right hand side of equation (5.20) relates to the uncertainty in thermal expansion coefficient:

$$u^2(\alpha)\, L^2\, (\Delta t)^2. \tag{5.21}$$

For steel GB, the uncertainty of thermal expansion coefficient is taken as $u(\alpha) = 5\times10^{-7}\ \text{K}^{-1}$. The average of measured temperature difference from the

reference temperature Δt is - 0.2°C for the DEI measurements. Substituting these values in equation (5.21), then:

$$u(\alpha)\, L\, \Delta t = -1.0\times 10^{-7}\, L. \tag{5.22}$$

The second term on the right hand side of equation (5.20) corresponds to the uncertainty in GB temperature measurement:

$$\alpha^2 L^2 u^2(\Delta t). \tag{5.23}$$

When the thermal expansion coefficient of steel GBs α is 11.6×10^{-6} K^{-1}.and the combined uncertainty for temperature measurements is given as 7 mK, then:

$$\alpha\, L\, u(\Delta t) = 8.1\times 10^{-8}\, L \tag{5.24}$$

5.3.3 Uncertainty Evaluation of l_A

Uncertainty attributed to non-ideal optics and wavefront aberrations is estimated using the DEI by repeating measurements without a GB as shown in Figure 5.1.

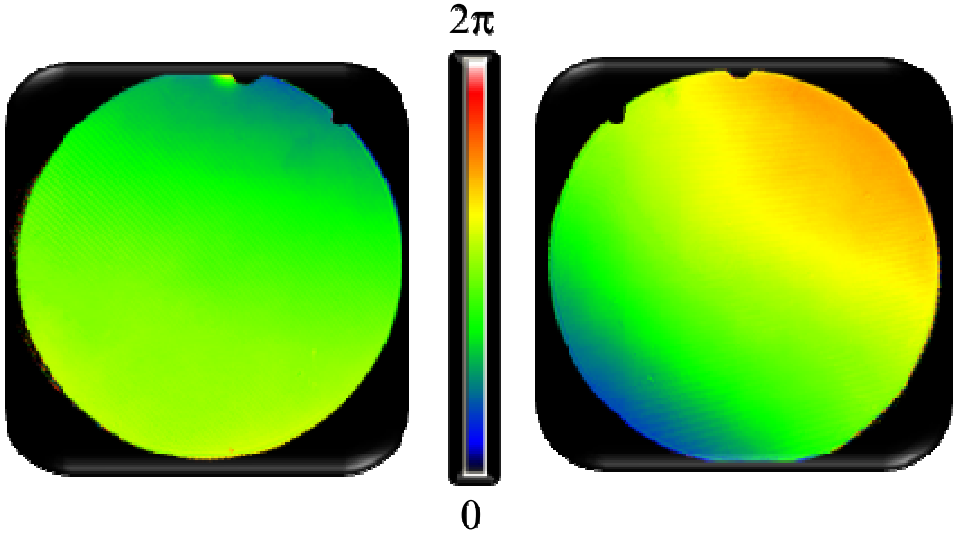

Figure 5.1 Phase maps of the DEI in both arms when GB is absent.

$$u(l_A) = 5 \text{ nm},$$

where the sensitivity coefficient is equal to 1. The largest contribution of the optics errors is due to the first collimator (no. 5 in Figure 3.1), which causes chromatic aberration (failure of a lens to focus all colours to the same focal point). The influence of the two reference mirrors of both arms (no. 12 in Figure. 3.1) would cancel if there were perfectly flat. In fact the reference mirrors are specified with a flatness error less than λ/20. This error is neglected, which is justified by the measurement of the empty interferometer shown in Figure 5.1.

5.3.4 Uncertainty Evaluation of l_Ω

The fiber end is considered as the light source of the interferometer because the end of the fiber is exactly placed at the focal point of the collimator. Thus, there is an obliquity effect as a result of the finite size of the source. The combined standard uncertainty is evaluated by partial derivative of equation (5.7). Hence:

$$u_c^2(l_\Omega) = \left(\frac{aL}{8f^2}\right)u^2(a) + \left(\frac{-a^2L}{8f^3}\right)u^2(f), \tag{5.25}$$

where a is the source diameter and equal to 2.8 μm, f is the focal length of the collimator and equal to 800 mm, $u(a)$ is the uncertainty of the fiber diameter and taken as 0.03 μm and $u(f)$ is equal to 0.25 mm. When substituting these values in the equation (5.25):

$$u_c(l_\Omega) = 1.6\times10^{-14}L. \tag{5.26}$$

5.3.5 Uncertainty Evaluation of l_v

At PTB, l_v is assumed to be zero in optical interferometry due to the superior quality GBs. Slight deviations in GB geometry by non-flatness and non-parallelism are also a source of uncertainty. As shown in Figure 5.2 [47], for the central length measurement, non-parallelism has an effect larger than a deviation from non-flatness.

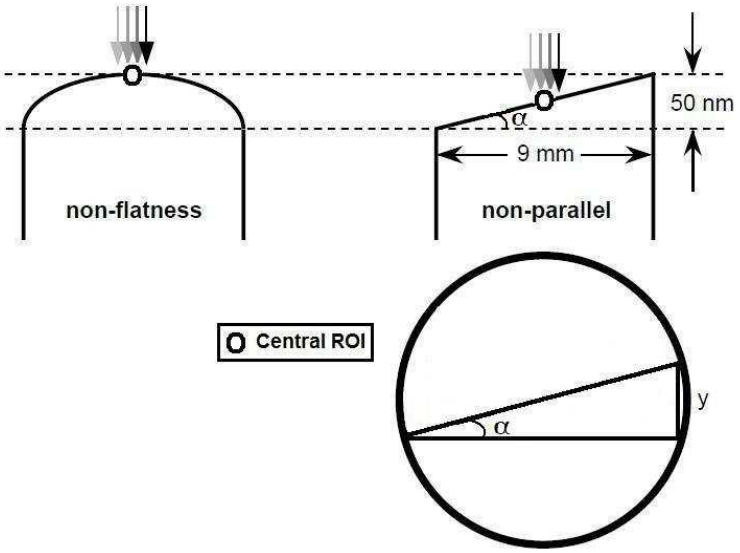

Figure 5.2 The non-parallelism and non-flatness properties of a GB. The effect of non-parallelism is larger than the effect of non-flatness for central point length measurement, source: [47].

When calculating the uncertainty of non-parallelism and flatness values, the central ROI should be considered because the length of the GB is measured by taking care of the central region of the GB.

The uncertainty in defining the center of the GB surface is 0.5 mm and the central length difference for a 50 nm deviation in non-parallelism [43, 47] along the crosswise direction of the GB is:

$$\tan\alpha = \frac{50\,\text{nm}}{9\,\text{mm}} = \frac{y}{0.5\,\text{mm}}, \tag{5.27}$$

y is equal to 2 nm which is the uncertainty term for variation in length for one face. Sensitivity coefficient for this term is 1. When DEI is used, this value is doubled considering the two faces of the GB.

$$u\ (l_v) \cong 4\ \text{nm}$$

5.3.6 Uncertainty Evaluation of l_ϕ

In PTB, the uncertainty contribution of GB phase correction can be taken as 4 nm for surface roughness and 3 nm for phase change on reflection [49]. When DEI is used, this value is doubled considering the two faces of the GB as given in table 5.4.]. The given value for the uncertainty of the phase change on reflection is in agreement with experimental results done using the DEI.

5.4 DEI Uncertainty Table

Standard uncertainty component	Source x_i	Standard uncertaint y $u(x_i)$	Sensitivity coefficients $\delta f/\delta x_i$	Contribution to length uncertainty
$u_c(l_{fit})$	**Best fit length:**			
$u(q_k)$	Vacuum wavelength			
	He-Ne laser	$5\times10^{-11}\lambda_1$	$(1/2\ \lambda_1)L$	$2.5\times10^{-11}\lambda_1$
	Nd-YAG laser	$7\times10^{-12}\lambda_2$	$(1/2\ \lambda_2)L$	$3.5\times10^{-12}\lambda_2$
$u(\lambda_k)$	Combined uncertainty contribution to $(l_1+l_2)/2$			**$1.3\times10^{-11}\ L$**
	Fringe fraction			
	@ 633 nm	0.01 fringe	$\lambda_1/2$	3.2 nm
	@ 532 nm	0.008 fringe	$\lambda_2/2$	2.1 nm
	Combined uncertainty contribution to (11+12)/2			1.9 nm
$u_c(n_k)$	Uncertainty for both faces of the GB			**3.8 nm**
	Refractive index of air:			
	@ 633 nm	2×10^{-8}	$(1/\ n_1)L$	$2\times10^{-08}\ L$
	@ 532 nm	2×10^{-8}	$(1/n_2)L$	$2\times10^{-08}\ L$
	Combined uncertainty contribution to $(l_1+l_2)/2$			**$1.4\times10^{-08}\ L$**
$u_c(l_t)$	**Thermal effects:**			
$u(t_g)$	GB temperature	7 mK	$\alpha\ L$	**$8.1\times10^{-8}\ L$**
$u(\alpha)$	Coefficient of thermal expansion	$5\times10^{-07}\ K^{-}$	$\Delta t\ L$	**$-1\times10^{-7}\ L$**

Standard uncertainty component	Source x_i	Standard uncertainty $u(x_i)$	Sensitivity coefficients $\delta f/\delta x_i$	Contribution to length uncertainty
	Interferometer optics:			
$u_c(l_A)$	Optics error	5 nm	1	5 nm
	Obliquity Source size	30 nm	$5.47\times10^{-10}L$	$1.64\times10^{-14}L$
$u_c(l_v)$	GB flatness and parallelism:	4 nm	1	4 nm
$u_c(l_\phi)$	phase correction			
	phase change on reflection	6 nm	1	6 nm
	surface roughness:	8 nm	1	8 nm
	Combined Standard Uncertainty:			$u^2=(12\text{ nm})^2+(0.13\times10^{-6}\,L)^2$
	Expanded Uncertainty for Coverage Factor k=2:			$U=\sqrt{\{(12\text{nm})^2+(0.13\times10^{-6}\,L)^2\}}\}$

Table 5.4 PTB-DEI standard uncertainty components for steel GBs.

Chapter 6

Measurement Results

For the results to be presented in this thesis 18 steel GBs up to 500 mm and 4 ceramic GBs up to 40 mm were selected to be measured using the DEI.

6.1 Autocollimation Test

In order to evaluate the quality of the described autocollimation method in § 3.4, the length of a 100 mm steel GB is measured at defined misalignment angles. For this purpose the fiber end, which is placed in the focal point of the collimator, is displaced from its initial zero position by certain distances leading to the misalignment:

$$\theta - \theta_o = \frac{1}{f_{coll}} \sqrt{(x - x_o)^2 + (y - y_o)^2}\,, \tag{6.1}$$

in which f_{coll} is the focal length of the collimator, x_o, y_o and θ_o identify the deviations from the ideal perpendicular incidence in the zero position. Due to the cosine error, the length $\bar{l}$ is expected to be measured shorter compared to the actual length, l:

$$\bar{l} = l \cos[\theta - \theta_o] \overset{\theta - \theta_o << 1}{\cong} l\left[1 - \tfrac{1}{2}(\theta - \theta_o)^2\right]. \tag{6.2}$$

Figure 6.1 shows the resulting systematic decrease of the measured lengths. Data points indicated by circles are obtained with the green laser, whereas the

squares represent results taken with the red laser. Data points are fitted according to equation 6.2 with x_o and y_o as free parameters and f_{coll} = 800 mm. For the data set shown in Figure 6.1 the resulting values, indicating the positions of the maxima, are x_o = -61 µm, y_o = -56 µm with θ_o = 0.104 mrad (green laser) and x_o = -34 µm, y_o = -43 µm with θ_o = 0.07 mrad (red laser). Accordingly, the cosine error at zero position of the fiber is well below 1 nm. This result illustrates the good quality of the auto-collimation adjustment described above.

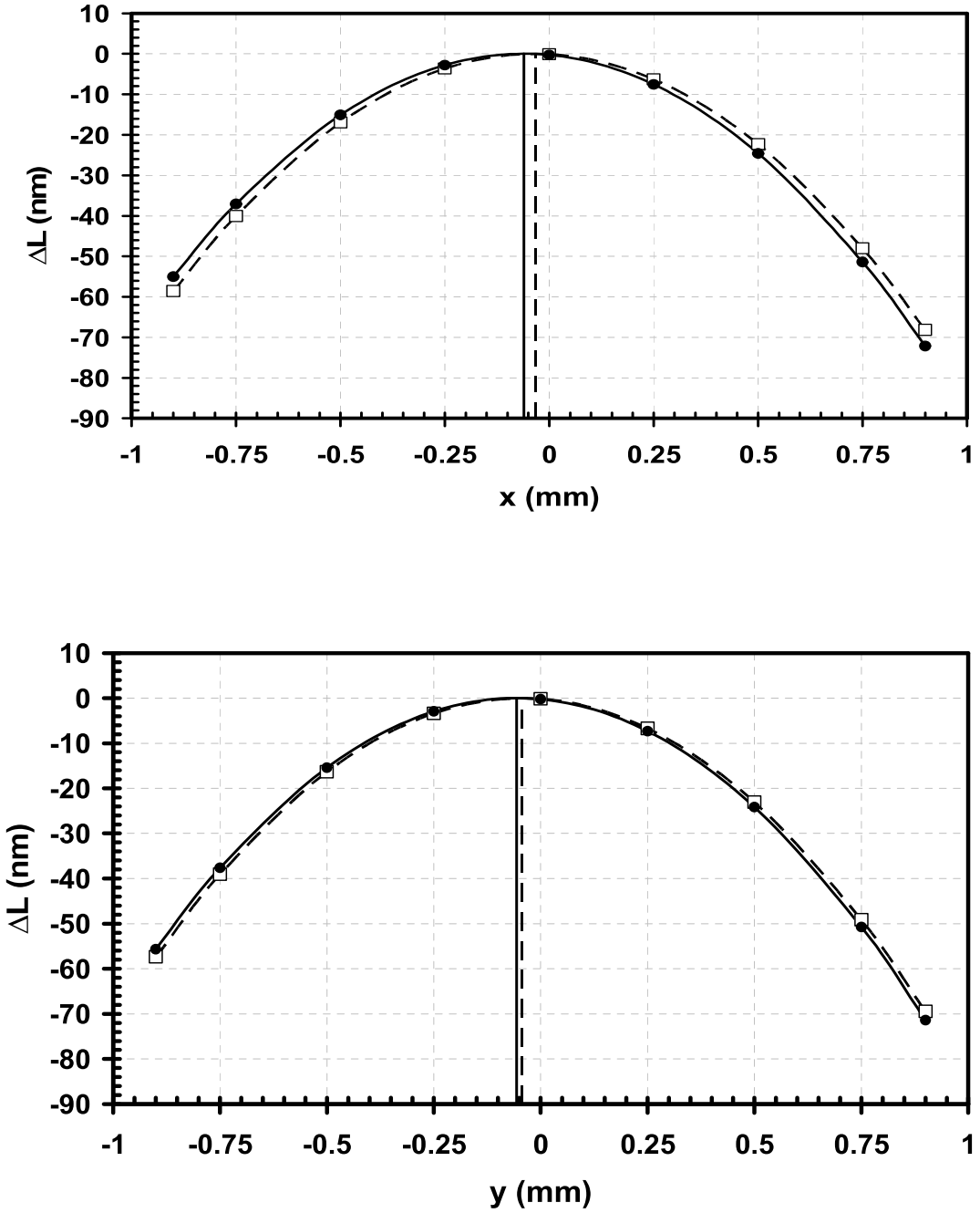

Figure 6.1 Length evaluation at different x and y positions of the fiber output, where the zero positions are based on autocollimation with the green laser (532 nm): circles, measurement points with the green laser fitted by the solid curves; squares, measurement points with the red laser (633 nm) fitted by the dashed curves.

6.2 The Effect of using Two Different Wavelengths

Figure 6.2 shows, for a set of samples, that the coincidence between the results obtained with the two different laser wavelengths is typically better than 2 nm.

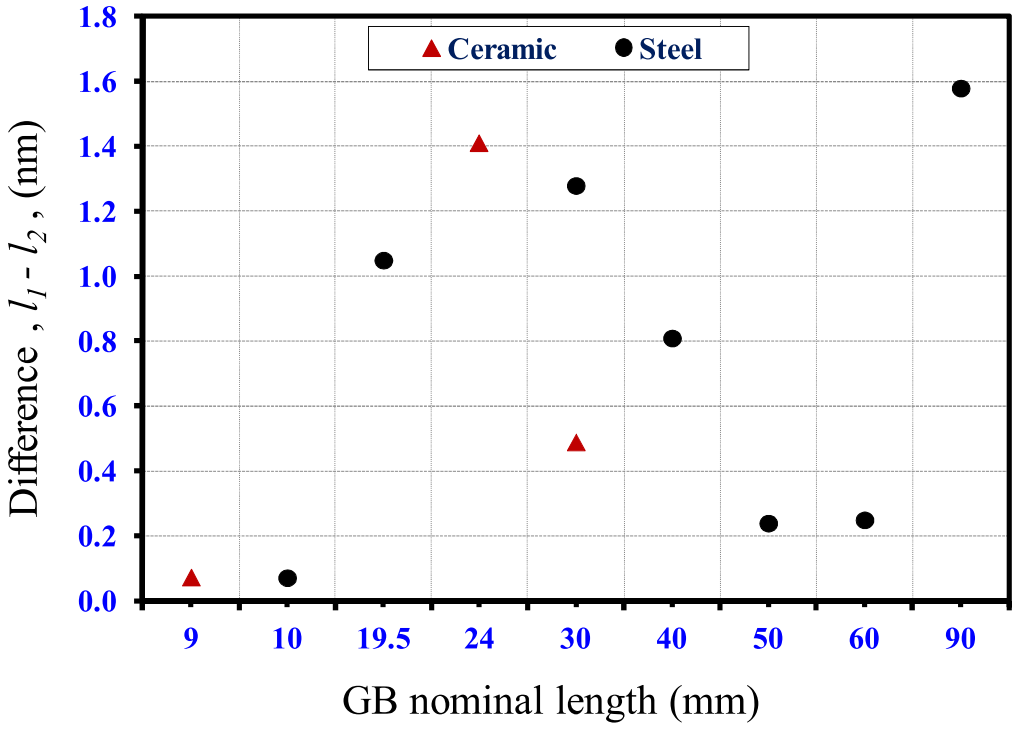

Figure 6.2 Coincidence between the lengths measured with two different wavelengths for a set of steel GBs.

6.3 Repeatability of the DEI measurements

For a 10 mm and a 300 mm steel GB, after correcting the lengths measured by the DEI to 20°C using equation (4.18) and adding the phase correction, described in § 4.5.2, the repeatability of the DEI measurements is less than 3

nm, as shown in Figure 6.3, where the phase correction for the 10 mm GB is 42 nm and for the 300 mm GB is 52 nm, the difference between these two values is due to the different surface roughness of the two GBs.

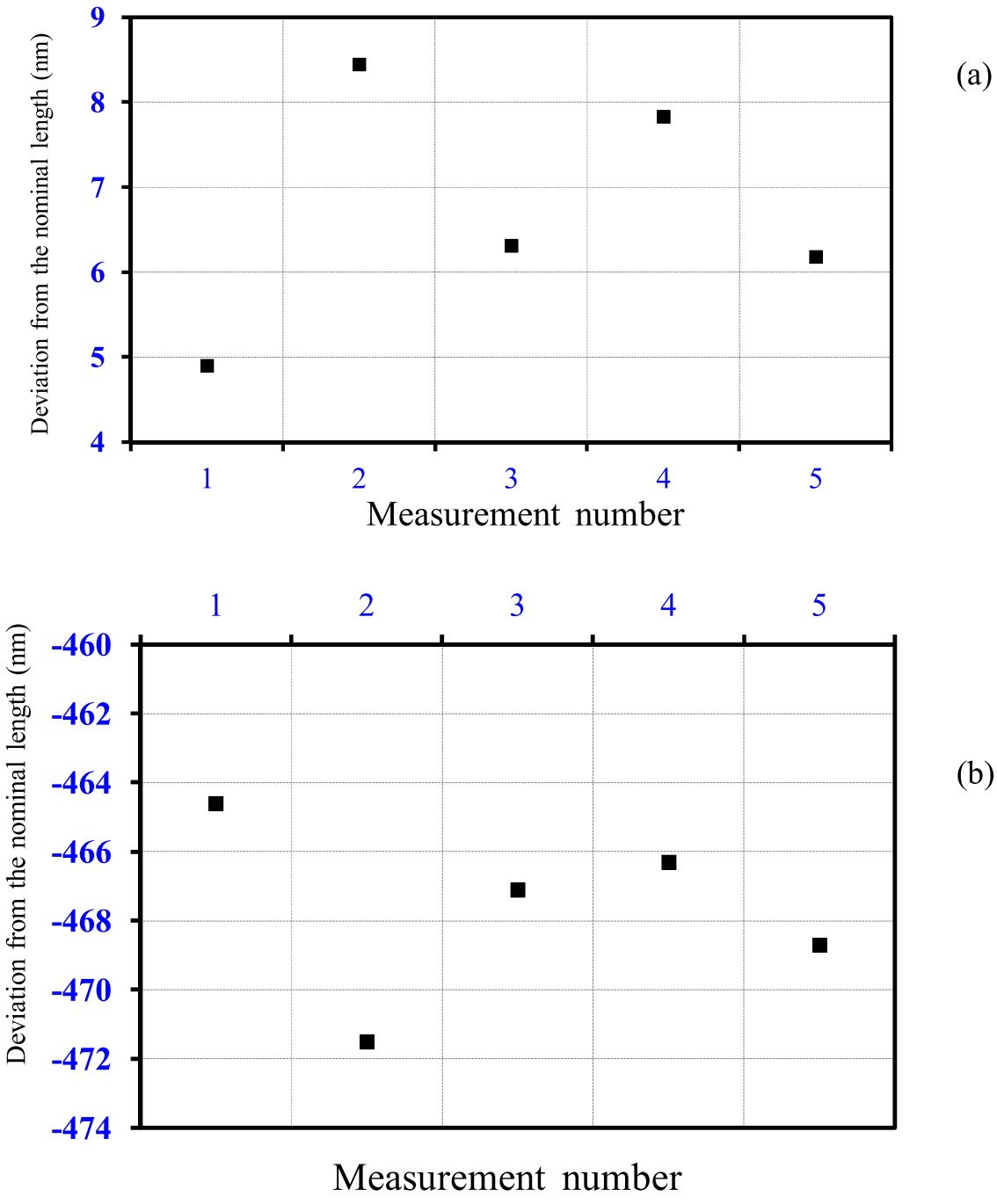

Figure 6.3 Deviation of DEI measurements from nominal length for two steel GBs, 10 mm (a) and 300 mm (b).

6.4 Comparison between the DEI and SEIs

According to the DEI standard uncertainty components for steel GBs shown in Table 5.4, the maximum difference between all measurements performed with the DEI and PTB's SEIs, is within the stated measurement uncertainty as illustrated by Figure 6.4.

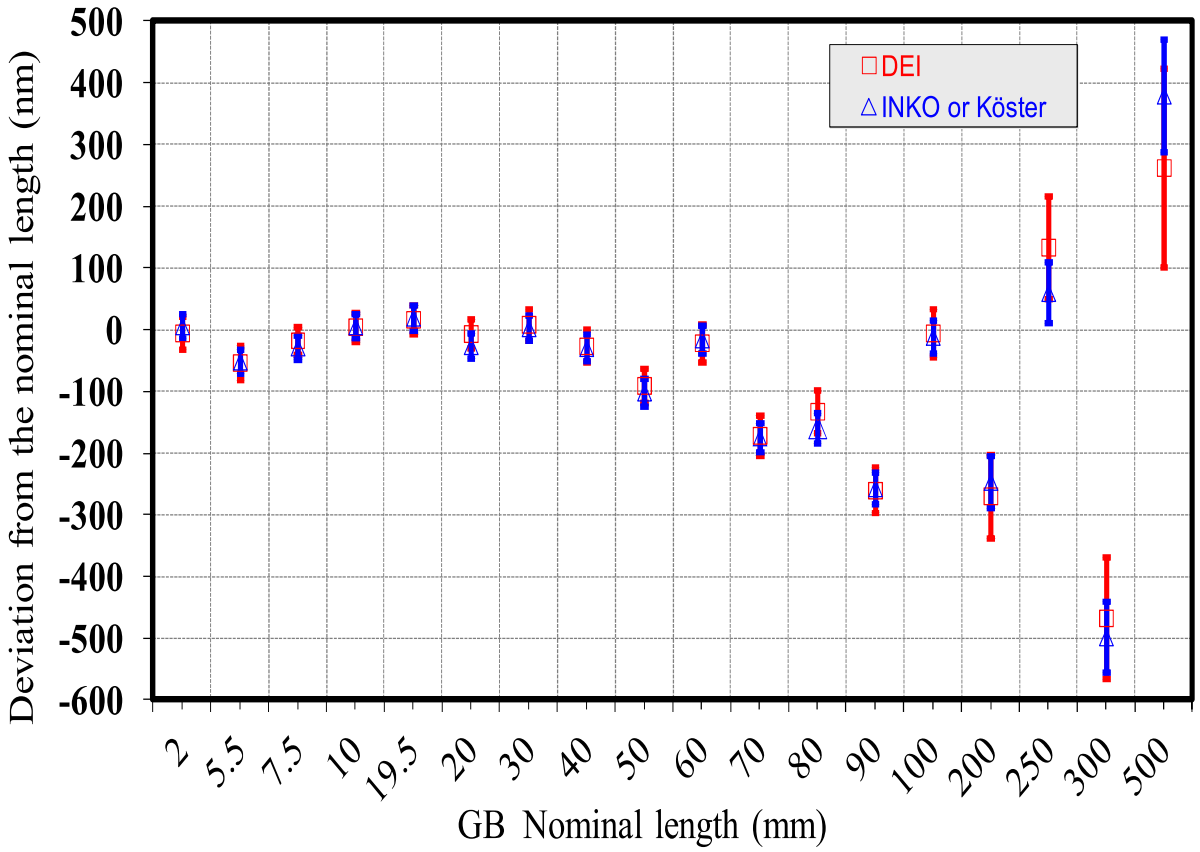

Figure 6.4 Length measurements and individual measurement uncertainty for the 18 steel GBs measured with the DEI (squares) and INKO5 or Köster (triangles) interferometers.

6.5 Determination of Phase Change on Reflection of Steel GB

The phase change on reflection is measured experimentally using the method of stack experiments. Five short steel GBs of nominal lengths 2 mm, 5.5 mm, 7.5 mm, 10 mm and 40 mm with known surface roughness are selected to be used in the pack (or stack) experiment [47, 50, 51]. First, each GB is measured individually, then wringing them together into a pack and measuring the pack by the same way as of individual GB.

To obtain good accuracy of the results, the stack method is applied in five sets as given below:

1) 10 mm and 7.5 mm,
2) 10 mm, 7.5 mm and 5.5 mm,
3) 10 mm, 7.5 mm, 5.5 mm and 2 mm,
4) 7.5 mm, 5.5 mm and 2 mm
5) 10 mm and 40 mm.

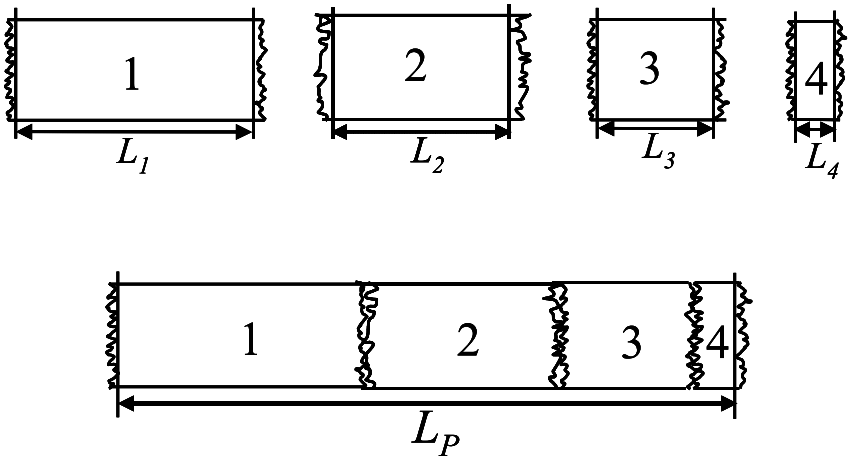

Figure 6.5 Stack method for four GBs.

For each set GBs, virtual length difference l_ϕ caused by the optical parameters n and κ is calculated from the difference in the measured length of the pack l_P and the sum of the measured lengths individually. Then the measured phase change on reflection l_ϕ can be expressed as:

$$l_\phi = \frac{1}{2m-2}\left[l_p - \left(\sum_{i=1}^{m} l_i + \sum_{i=1}^{m-1} S_i^R + \sum_{i=2}^{m} S_i^L \right) \right], \tag{6.3}$$

where l_p represents the measured length of the pack, l_i is the measured lengths of the m individual gauges making up the pack and S_i^R, S_i^L are the measured surface roughness for the right end and the left end of GB respectively .

The measured values for the phase change on reflection of steel gauge surface, obtained by applying the stack method are summarized in Table 6.1.

GB Set	**Phase Change on Reflection (nm)**
10 mm and 7.5 mm	26
10 mm, 7.5 mm and 5.5 mm	23
10 mm,7.5 mm, 5.5 mm and 2 mm	26
7.5 mm, 5.5 mm and 2 mm	21
10 mm and 40 mm	21
Average value	**23.8**

Table 6.1 The phase change on reflection for steel GB.

Thus, the average value for steel phase change on reflection measured using the DEI agrees with the calculated values shown in Table 6.1.

6.6 Determination of Phase Correction of Ceramic GB

For the four ceramic GBs, the average difference between the measured lengths of the two interferometers (DEI and INKO5), shown in table 6.2, is 65 nm which can be interpreted as the phase correction value. On the other hand, using the DEI, the stack method experiment was applied for 9 mm and 24 mm ceramic GBs with phase correction value of 69 nm.

Nominal length	Manufacture	Identification number	$L_{measured}$ using DEI (nm)	$L_{measured}$ using INKO (nm)	L_{DEI}-L_{INKO} (nm)
9 mm	TESA	A09909	54	133	-79
24 mm	Mitutoyo	872006	155	195	-40
30 mm	TESA	A02910	037	111	-74
40 mm	Mitutoyo	920329	-150	-082	-68
				Average value	**-65 nm**

Table 6.2 The measured lengths of four ceramic GBs using DEI and SEI.

These two values of the phase correction, 65 nm and 69 nm, agree with the phase correction values reported in Ref. [50, 51]. In Ref.[50] a phase shift of 20.5 nm and a surface roughness of 10 nm are reported for a single face of a ceramic GB, i.e., a value of 61 nm for the overall phase correction of two faces would be expected, while in Ref.[51] 47 nm phase correction is used when ceramic GB is wrung to a quartz platen. Thus, it is concluded that the phase correction of ceramic GB can be measured well using the DEI.

Chapter 7

Summary and Outlook

The work presented in this thesis describes a prototype version of a double-ended interferometer (DEI) built at Physikalisch-Technische Bundesanstalt (PTB) for measuring the length of short as well as long gauge blocks (GBs).

In this setup, more than one wavelength is used which makes this interferometer much more effective for accurate extraction of the integer orders of interference. A special design for the light source is found to allow the same adjustment states at the different wavelengths.

The PTB-DEI prototype shows consistent results for the two wavelengths used and a good agreement with well-established PTB GB interferometers (INKO5 and Köster). The current uncertainty of the DEI prototype is limited by the GB temperature deviation from the reference temperature of 20.000 °C.

The phase change on reflection of steel GBs is measured using the stack method. It shows a good agreement with the calculated ones.

The phase correction of ceramic GB is determined from the difference between the DEI and the INKO5 measurement results and is measured using the stack method. Its value is compatible with the values reported in the literature using the same method.

The good experimental results introduce this interferometer as a traceable tool for other GB length interferometers.

All the knowledge, experience and results acquired from this prototype will be used to build the final DEI setup which will be situated in a temperature controlled vacuum chamber as other specialized precision interferometers at PTB [52, 53].

Chapter 8

References

[1] Joint Committee for Guides in Metrology (JCGM), "International Vocabulary of Metrology Basic and General Concepts and Associated Terms" 3 rd ed., 200, Sevres, France, (2008).

[2] H. S. Nielsen, "Taking Dimensional Metrology to the Next Level", international dimensional metrology workshop (IDW), Nashville, USA, (2005).

[3] http://en.wikipedia.org/wiki/Cubit.

[4] A. J. Lewis, "Absolute Length Measurement using Multiple-Wavelength Phase Stepping Interferometry", Ph. D. Thesis, University of London (1993).

[5] T. Doiron, J. Beers, "The Gauge Block Handbook", National Institute of Standards and Technology (NIST), Monograph 180, (2005).

[6] P. Giacomo, "The New Definition of the Metre", Am. J. Phys. 52, pp. 607-613, (1984).

[7] H. Barrell, "The Metre", Contemporary Phys. vol. 3, pp. 415-434, (1962).

[8] P. Franke, R Schödel, " Interferometrische Kalibrierung von Parallelendmaßen ", PTB-Mitteilungen 120, 1, (2010).

[9] F. Twyman, A. Green, “Prisms and Microscopes”, British patent no 103832, (1916).

[10] W. Kösters, “Prüfung von Johansson-Endmassen mit Lichtinterferenz” Feinmechanik (Präzision) 1, pp. 2-5, (1920), and pp. 39-41, (1922).

[11] J. H. Dowell, “Improvements in or Relating to Interferometers for Determination of Length”, British patent no. 555672, (1943).

[12] P. Hariharan, D. Sen, “New Gauge Interferometer”, Journal of the optical society of America, vol. 49, issue 3, pp. 232-234, (1959).

[13] K. Dorenwendt, “Interferentielle Messung von nicht angeschobenen Endmaßen”, PTB Annual Report 1972, pp. 121, (printed 1973).

[14] V. M. Khavinson and L. F. Khavinson, “Two-side interferometer for measuring the length of gauge blocks,” in Investigations in the Field of Length and Angle Measurements, Proceedings of the D. I. Mendeleyev Institute for Metrology, N. P. Gerasimov, ed. (Energoatomizdat, Leningrad, Russia), pp. 14–18 (1983).

[15] V. M. Khavinson, “Ring Interferometer for Two-Sided Measurement of the Absolute Lengths of End Standards”, Appl. Opt. 38, pp. 126-135, (1999).

[16] Y. Ishii, S. Seino, “New Method for Interferometric Measurement of Gauge Blocks without Wringing onto a Platen”, Metrologia 35, pp. 67-73, (1998).

[17] S. H. Lu, C. Chiueh, C. Lee, “Measuring the Thickness of Opaque Plane-Parallel Parts using an External Cavity Diode Laser and a Double-Ended Interferometer”, Optics Communications 226, pp. 7-13, (2003).

[18] Y. Kuriyama, Y. Yokoyama, Y. Ishii , J. Ishikawa, “Development of a New Interferometric Measurement System for Determining the Main Characteristics of Gauge Blocks”, Annals of the CIRP vol. 55/1, (2006).

[19] Mitutoyo company, Gauge Block with Calibrated Coefficient of Thermal Expansion (CTE), Catalog No. E4334.

[20] M. Born, E. Wolf, “Principles of Optics”, 6th ed. New York, (1989).

[21] B. Karlsson, C.G. Ribbing, “Optical Constants and Spectral Selectivity of Stainless Steel and its Oxides”. J. Appl. Phys. 53, Issue 9, 6340- 6346, (1982).

[22] R. Schödel, Chapter 15: “Length and Size, Handbook of optical Metrology: Principles and applications”, T. Yoshizawa; Saitama University, Japan, (2009).

[23] G. Bönsch, “Gauge Blocks as Length Standards Measured by Interferometry or Comparison Length Definition, Traceability Chain, and Limitations”, SPIE vol. 3477, pp. 199-210, (1998).

[24] G. Bönsch, “Interferometric Calibration of an Integrating Sphere for Determination of the Roughness Correction of Gauge Blocks” Proc. SPIE 3477, pp. 152-160, (1998).

[25] Bureau Internatinal des Poids et Mesures (BIPM), “Iodine (λ ≈ 633 nm) Absorbing Molecule $^{127}I_2$, a_{16} or f Component, R (127) 11-5 Transition”, (2003).

[26] Bureau Internatinal des Poids et Mesures (BIPM), “Iodine (λ ≈ 532 nm) Absorbing Molecule $^{127}I_2$, a_{10} Component”, R (56) 32-0 Transition”, (2003).

[27] H. Matsumoto, T. Honda, “High Accuracy Length-Measuring Interferometer using the Two-Colour Method of Compensating for the Refractive Index of Air”, Meas. Sci. Technol. 3, pp. 1084-1086 (1992).

[28] Schäfter + Kirchhoff company, Optical scheme of beam combiner 2 to 1 with Shutter, (2009).

[29] Schäfter + Kirchhoff company, Multicube data sheet, (2011)

[30] Micos company, Motion control system, Technical Report, vol. 9.

[31] Physik Instrumente company, Piezo nano position catalog, (2009).

[32] Paroscientific Int, Digiquartz pressure instrumentation company, Model 745 data sheet, (2005).

[33] Testo company, “Stationary Measurement Solutions, Transmitters and monitoring systems”, (2011).

[34] T. M. Gruhn, “Vollautomatische Kalibrierung von Parallelendmaßen mit Hilfe der Phasenverschiebungsinterferometrie”, Ph. D. Thesis, Technical University of Braunschweig, (2003).

[35] B. Edlèn, “The Refractive index of Air”, Metrologia, 2, pp. 71-80, (1966).

[36] G. Bönsch, J. R. Potulski, “Measurement of the Refractive Index of Air and Comparison with Modified Edlèn’s Formulae”, Metrologia 35, pp. 133-139, (1998).

[37] P. Giacomo, “Equation for the Determination of the Density of Moist Air”, Metrologia, 18, pp. 33-40, (1982).

[38] R. S. Davis, “Equation for the Determination of the Density of Moist Air” (1981/91)”, Metrologia 29, pp. 67-70, (1992).

[39] H. Darnedde, “High Precision Calibration of Long Gauge Blocks using the Vacuum Wavelength Comparator”, Metrologia, 29, pp. 349-359, (1992).

[40] J. E. Decker, J. R. Pekelsky, “Gauge Block Calibration by Optical Interferometry at the National Research Council of Canada”, Measurement Science Conference Pasadena NRC, international report no. 40002, (1997).

[41] S. Tang, “Self-Calibrating Five Frame Algorithm for Phase Shifting Interferometry”, SPIE, Vol. 2860, (1991).

[42] R. Schödel and J. E. Decker “Methods to Recognize the Sample Position for Most Precise Interferometric Length Measurements”, Proc. of SPIE, vol. 5532, (2004).

[43] International Organization for Standardization (ISO), ISO 3650-1978 (E), “ISO Standards Handbook 33: Applied Metrology Limits, Fits and Surface Properties”, 1st ed., (1998).

[44] International Organization for Standardization (ISO), “Guide to the Expression of Uncertainty in Measurement”, 1st ed., (1993), corrected and reprinted (1995).

[45] United Kingdom Accreditation Service (UKAS), “The Expression of Uncertainty and Confidence in Measurement”, ed. 2, (2007).

[46] European Co-operation for Accreditation (EA), “Expression of the Uncertainty of Measurement in Calibration”, EA-4/02, (1999).

[47] J. E. Decker, J. R. Pekelsky, “Uncertainty Evaluation for the Measurement of Gauge Blocks by Optical Interferometry”, Metrologia, 34, pp. 479-493, (1997).

[48] D. S. Cuhadar, “The Köster’s Interferometer for Gauge Block Length Measurements”, Ph. D. Thesis, Middle East Technical University, Turkey, (2007).

[49] J. E. Decker, R. Schödel, G. Bönsch, “Considerations for the Evaluation of Measurement Uncertainty in Interferometric Gauge Block Calibration Applying Methods of Phase Step Interferometry”, Metrologia 41, pp. L11–L17, (2004).

[50] S. Shutoh, H. Moriyama, M. Sawabe, “Phase Shift on Ceramic Gauge Blocks” Proc. SPIE 3477, pp.181-186, (1998).

[51] J. E. Decker, A. Lapointe, J. Stoup, M. Viliesid Alonso, J. R. Pekelsky, “NORAMET Comparison of Gauge Block Measurement by Optical Interferometry”. Metrologia 36, pp. 421-432, (1999).

[52] R. Schödel, “Ultra High Accuracy Thermal Expansion Measurements with PTB’s Precision Interferometer”, Meas. Sci. Technol. 19, 084003, (2008).

[53] R. Schödel, A. Walkov, “Das Neu Aufgebaute Ultrapräzisions Interferometer”, PTB-Mitteilungen: 120, 1, (2010).